# The $s$-version of Finite Element Method for Laminated Composites

**Jacob Fish  Ravi Guttal**
Department of Civil Engineering and Scientific Computation Research Center,
Rensselaer Polytechnic Institute, Troy, NY 12180. U.S.A

**Abstract**

The $s$-version of finite element method is developed for laminated plates and shells. By this technique the global domain is idealized using 2D Equivalent Single Layer model. The regions where ESL model errs badly in capturing localized phenomena are superimposed by a stack of 3D elements. Assumed strain formulation and selective polynomial order escalation in the two models as well as fast iterative procedures are employed to maintain high level of computational efficiency.

## 1. Introduction

Laminated composites present to the analyst a hard nut to crack due to inadequacy of Equivalent Single Layer (ESL) theories in resolving 3D phenomena on one hand and computational complexity of layer-wise or 3D models on the other hand. A natural remedy is a global local approach in which different regions of the problem domain are described with different types of models. We refer to [21] for comprehensive review of global-local techniques for composite laminates and to [6] and [7] for various aspects of reliability, convergence and accuracy of global-local techniques.

Here we focus only on the class of global-local techniques that advocates hierarchical solution strategy in the sense that information from the analysis of an ESL model is exploited in resolution of local effects using Discrete Layer (DL) mesh. Among the most popular hierarchical global-local strategies are various forms of multigrid and composite grid methods [13]-[18], as well as methods based on hierarchical decomposition of approximation space [1]-[5], [19]-[21]. Recently the composite grid method originated for displacement-based linear systems has been extended to hybrid systems[25]. Engineering global-local approaches which approximate a detailed response by means of post processing techniques, such as subjecting refined discrete layer model to the boundary conditions extracted from the global ESL model, can be viewed as a single iteration within the composite grid procedure. For various improvements of this simple "zoom" technique we refer to [22][23][24].

The present paper is an extension of our previous work on the $s$-version of the finite element method in 2D [1] [4] to laminated plates and shells. In this paper we emphasize the utility of the mesh superposition technique to:

- Identify the location of the critical regions where DL model is needed using Dimensional Reduction Error (DRE) indicators.
- Accurately and efficiently predict both local and global effects using assumed strain formulation, selective polynomial order escalation and dedicated iterative solution procedures for hierarchical systems.

The outline of the paper is as follows: In section 2 the *s*-method is introduced in the context of laminated plates and shells. Assumed strain formulation and a novel quadrature scheme are briefly discussed in section 3. Dimensional Reduction Error indicators and quality control techniques are described in section 4. A brief discussion on the feasibility of iterative and direct solvers for the *s*-method is presented in section 5. Numerical examples conclude the manuscript.

# 2. Mesh superposition for laminated composites

Consider a heterogeneous medium on domain $\Omega$ with boundary $\Gamma$ as shown in Fig. 1. The boundary $\Gamma$ is decomposed as $\Gamma = \Gamma_u \cup \Gamma_t$, where $\Gamma_u$ is the boundary with prescribed displacements and $\Gamma_t$ with prescribed traction. The critical region to be superimposed by a local mesh is denoted by $\Omega^L$, $\Omega^L \subset \Omega$. Domains $\Omega$ and $\Omega^L$ are subdivided independently into element domains such that $\cup\Omega_e^G = \Omega$ and $\cup\Omega_e^L = \Omega^L$. Let $\Gamma^{GL}$ be the boundary between the two meshes such that $\Gamma \cap \Gamma^{GL} = \emptyset$. Let $\mathbf{u^G}$ be the global displacement field defined on $\Omega$ and $\mathbf{u^L}$ be the local displacement field defined on the local region $\Omega^L$. The total displacement field is constructed by superposition:

$$\mathbf{u} = \mathbf{u^G} + \mathbf{u^L} \tag{1}$$

In the case of laminated plates and shells, the global displacement field $\mathbf{u}^G$ is represented by the Equivalent Single Layer (ESL) model. The ESL model on $\Omega^G$ is discretized using a hierarchic degenerated plate/shell finite elements [5].

In the notation employed in this manuscript, indices $(1,2)$ correspond to inplane coordinates and index '3' corresponds to the transverse direction as shown in Fig. 1. The Greek subscripts represent the inplane spatial components (1,2) only. The lower case Latin subscripts indicate spatial components (1,2,3) except for subscripts $a$, $b$ and $e$ which are reserved for element numbers. Uppercase subscripts indicate degrees of freedom. Summation convention is employed for repeated indices unless otherwise specified.

The displacement field $\mathbf{u}^G$ is expressed in terms of mid-point translations $u_i^t(\xi_1, \xi_2)$ and mid-point rotations $\theta_\alpha(\xi_1, \xi_2)$ which are defined with respect to the fiber coordinate system as:

$$\left\{ \begin{array}{c} u_1^G \\ u_2^G \\ u_3^G \end{array} \right\} = \sum_{A=1}^{NMDS} N_A^G(\xi_1,\xi_2) \left\{ \begin{array}{c} u_{1A}^t \\ u_{2A}^t \\ u_{3A}^t \end{array} \right\} + \sum_{A=1}^{NMDS} N_A^G(\xi_1,\xi_2) \; \frac{\xi_3}{2} \; [-t\mathbf{e}_2^f, \; t\mathbf{e}_1^f]_{(\xi_1,\xi_2)} \left\{ \begin{array}{c} \theta_{1A} \\ \theta_{2A} \end{array} \right\} \tag{2}$$

Where $\{N_A^G\}$ are the hierarchic basis of the interpolation space $S^G(\Omega^G, p^G, q)$ (defined as in [5]), $p^G$ is the maximum inplane polynomial order, $q$ the polynomial order in

transverse direction and $\Omega^G = \Omega$. NMDS are the number of hierarchic modes in the superimposed mesh. Note that there is a fundamental difference between equation (2) and its iso-parametric counterpart. In the classical iso-parametric formulation the variable vector functions $\mathbf{e}_i^f(\xi_1, \xi_2)$ in equation (2) are replaced by a set of constant vectors $\mathbf{e}_i^f(\xi_1^A, \xi_2^A)$ representing the fiber coordinate system at the node $A$. The present formulation gives rise to an additional term in the displacement gradient evaluation, resulting from the derivatives of $\mathbf{e}_i^f$. For a detailed formulation of hierarchic degenerated plate/shell element see [5].

To resolve the localized phenomena a Discrete Layer model is superimposed in the critical region $\Omega^L$. The DL model is discretized in terms of 3D hierarchical $C^0$ continuous shape functions $\{N_i^L\}$, spanning the interpolation space $S^L(\Omega^L, p^L)$ (defined in [9]), where $p^L$ is the maximum polynomial order. Thus the local displacement field is expressed as:

$$u_m^L = \sum_{A=1}^{NMDS} N_{mA}^L a_A \tag{3}$$

where $\mathbf{a}$ is the displacement vector representing the amplitudes of the hierarchic modes in the superimposed mesh.

To satisfy the $C^0$ displacement compatibility between the global (ESL) and local (DL) meshes, the following homogeneous boundary conditions are imposed on the local mesh at the boundary between the two meshes($\Gamma^{GL}$):

$$u_\alpha^L = 0 \ \ on \ \ \Gamma^{GL} \alpha \in [1,2] \tag{4}$$

where $\alpha$ corresponds to the inplane coordinates of the shell. Note that the local displacement field is not constrained in the transverse ($X_3$) direction on $\Gamma^{GL}$ as the underlying shell model has no extension mode in this direction. These constraints are equivalent to the so called telescopic constraints in finite element jargon.

The inhomogeneous displacement boundary conditions $\mathbf{u}^P$ on $\Gamma_u$ can be approximated with the global mesh, although better resolution of prescribed fields can be obtained by prolongating the remainder of the field

$$\mathbf{u}^L = I^L(\mathbf{u}^P - \mathbf{u}^{PG}) \ \ on \ \ \Gamma_u \tag{5}$$

to the local mesh [1]-[6]. In (5) $I^L$ is the prolongation operator from the local to global mesh and $\mathbf{u}^{PG} = \mathbf{u}^G$ on $\Gamma_u$.

To demonstrate the basic structure of the discrete equations, a linear elastostatics problem is considered. The discrete equations are obtained using Galerkin approximation of the weak form which states:
Given the spaces,

$$\begin{aligned}
U^G &= \{\mathbf{u}^G | \mathbf{u}^G \in S^G(\Omega^G, p^G, q, l^G);\ \mathbf{u}^G \in C^0(\Omega^G);\ \mathbf{u}^G = \mathbf{u}^{PG} \ on \ \Gamma_u\} \\
W^G &= \{\mathbf{w}^G | \mathbf{w}^G \in S^G(\Omega^G, p^G, q, l^G);\ \mathbf{w}^G \in C^0(\Omega^G);\ \mathbf{w}^G = 0 \ on \ \Gamma_u\} \\
U^L &= \{\mathbf{u}^L | \mathbf{u}^L \in S^L(\Omega^L, p^L, l^L);\ \mathbf{u}^L \in C^0(\Omega^L);\ \mathbf{u}^L = I^L(\mathbf{u}^P - \mathbf{u}^{PG}) \ on \ \Gamma_u;\ u_\alpha^L = 0 \ on \ \Gamma^{GL}\} \\
W^L &= \{\mathbf{w}^L | \mathbf{w}^L \in S^L(\Omega^L, p^L, l^L);\ \mathbf{w}^L \in C^0(\Omega^L);\ \mathbf{w}^L = 0 \ on \ \Gamma_u;\ w_\alpha^L = 0 \ on \ \Gamma^{GL}\}
\end{aligned} \tag{6}$$

where $\alpha \in [1,2]$ and $i \in [1,3]$.
Find

$$\mathbf{u}^G \in U^G,\ \mathbf{u}^L \in U^L, \mathbf{u} = \mathbf{u}^G + \mathbf{u}^L \tag{7}$$

such that for all $\mathbf{w}^G \in W^G,\ \mathbf{w}^L \in W^L, \mathbf{w} = \mathbf{w}^G + \mathbf{w}^L$

$$a(\mathbf{w}^G + \mathbf{w}^L,\ \mathbf{u}^G + \mathbf{u}^L)_\Omega = (\mathbf{w}^G + \mathbf{w}^L,\ b_i)_\Omega + (\mathbf{w}^G + \mathbf{w}^L,\ t_i)_\Gamma \tag{8}$$

where $S^G$ is the aforementioned interpolation space for the global domain $\Omega^G$, and $l^G$ is the list of active degrees of freedom to be determined in the adaptive process on the basis of the contribution of the corresponding basis functions towards reduction of discretization errors (Section 4). Similarly $S^L$ is the interpolation space for the local domain $\Omega^L$ and $l^L$ is the corresponding list of active degrees of freedom determined adaptively. $b_i$ and $t_i$ are prescribed body and traction forces respectively. $a(\cdot,\cdot)$, and $(\cdot,\cdot)$ are bilinear symmetric forms defined by

$$a(\mathbf{P},\mathbf{Q}) = \int_\Omega P_{(i,j)} D_{ijkl} Q_{(i,j)} d\Omega \tag{9}$$

$$(\mathbf{P},\mathbf{Q})_\Gamma = \int_\Gamma P_i\, Q_i d\Gamma \tag{10}$$

$$(\mathbf{P},\mathbf{Q})_\Omega = \int_\Omega P_i\, Q_i d\Omega \tag{11}$$

$D_{ijkl}$ is the constitutive tensor. The parenthesis about lower case subscripts designate the symmetric part of a second order tensor.

Discrete equations are obtained by substituting interpolants (2,3) for the both trial and test functions into the weak form (8) and requiring arbitrariness of the local and global variations. The structure of the resulting equation is given as:

$$\mathbf{K}\,\mathbf{d} = \mathbf{f} \tag{12}$$

where

$$\mathbf{K} = \begin{bmatrix} K^G_{AD} & K^C_{AE} \\ K^C_{BD} & K^L_{BE} \end{bmatrix} \quad \mathbf{d} = \begin{Bmatrix} d_D \\ a_E \end{Bmatrix} \quad \mathbf{f} = \begin{Bmatrix} f^{ext}_A \\ h^{ext}_B \end{Bmatrix} \tag{13}$$

and,

$$K^G_{AD} = a(\mathbf{N}^G_A, \mathbf{N}^G_D) = \int_\Omega B^G_{ijA} \hat{D}_{ijkl} B^G_{klD} d\Omega \tag{14}$$

$$K^L_{BE} = a(\mathbf{N}^L_B, \mathbf{N}^L_E) = \int_{\Omega^L} B^L_{ijB} D_{ijkl} B^L_{klE} d\Omega \tag{15}$$

$$K^C_{AE} = a(\mathbf{N}^G_A, \mathbf{N}^L_E) = \int_{\Omega^L} B^G_{ijA} D_{ijkl} B^L_{klE} d\Omega \tag{16}$$

$$f^{ext}_A = (N^G_A, \mathbf{b})_\Omega + (N^G_A, \mathbf{t})_{\Gamma_t} = \int_\Omega N^G_{iA} b_i d\Omega + \int_\Gamma N^G_{iA} t_i d\Gamma \tag{17}$$

$$h^{ext}_B = (N^L_B, \mathbf{b})_{\Omega^L} + (N^L_B, \mathbf{t})_{\Gamma_t} = \int_{\Omega^L} N^L_{iB} b_i d\Omega + \int_\Gamma N^L_{iB} t_i d\Gamma \tag{18}$$

$\mathbf{B}^G$ and $\mathbf{B}^L$ are the strain-displacement matrices corresponding to the ESL and DL models, respectively. The $\mathbf{B}$-matrix is modified using assumed strain method [10]

to enhance the element performance as described in the next section. Effective (or smeared) laminate material properties $\hat{D}_{ijkl}$ are used for calculation of global stiffness matrix and plane stress assumption is incorporated in $\Omega \backslash \Omega^L$. 3D material properties are used for the matrices in the local region.

To maintain rank sufficiency of the stiffness matrix $\mathbf{K}$ the global and local interpolation spaces must be mutually exclusive. For structured mesh superposition ($S_s$-version of FEM [1]) exclusively considered here, this can be accomplished explicitly as demonstrated below:

From the definition of spaces $S^G(\Omega^L, p^G, q)$ and $S^L(\Omega^L, p^L)$ it is evident that:

$$S^L(\Omega^L, p^L) \cap S^G(\Omega^L, p^G, q) \neq \emptyset \tag{19}$$

Hence redundant modes are encountered in the system (12), since a linear combination of underlying mesh basis functions can replicate a superimposed mesh basis function or vice versa.

Define an auxiliary space

$$\hat{S}(\Omega^L) \;=\; S^L(\Omega^L, p^L) \cap S^G(\Omega^L, p^G, q) \tag{20}$$

so that the rank sufficiency of the stiffness matrix $\mathbf{K}$ can be maintained using the following interpolation space

$$S(\Omega) \equiv S^G(\Omega^G, p^G, q) \cup \left( S^L(\Omega^L, p^L) \backslash \hat{S}(\Omega^L) \right) \tag{21}$$

or

$$S(\Omega) \equiv S^L(\Omega^L, p^L) \cup \left( S^G(\Omega^G, p^G, q) \backslash \hat{S}(\Omega^L) \right) \tag{22}$$

The two decompositions of the space $S(\Omega)$ (21,22) in the local region denoted by, $S(\Omega^L)$, represent a complete space of polynomial order $p^L$. The decomposition given in (21) is more convenient from the computational efficiency stand point because it allows to exploit previous computations in certain cases discussed in Section 5.

In order to construct the space $S(\Omega^L)$ we decompose it as a tensor product of two spaces:

$$S(\Omega^L) = S_{2D}(A^L, p_A^L) \otimes S_{1D}(T, t, p_t^L) \tag{23}$$

where $S_{2D}$ is spanned by 2D hierarchical basis of order $p_A^L$ [9] defined over the mid-surface of the shell over the local region $A^L$ and $S_{1D}^L$ is spanned by 1D hierarchical basis functions of order $p_t^L$ defined within each layer $t_i \subset T$, such that $\cup t_i = T$.

Each of the two spaces is constructed from a set of basis functions in the global and local meshes:

$$S_{2D}(A^L, p_A^L) \;=\; S_{2D}^G(A^L, p_A^G) \cup [S_{2D}^L(A^L, p_A^L) \backslash \hat{S}_{2D}^L(A^L)] \tag{24}$$

$$S_{1D}(T, t, p_t^L) \;=\; S_{1D}^G(t = T, q) \cup [S_{1D}^L(T, t, p_t^L) \backslash \hat{S}_{1D}^L(T, t)] \tag{25}$$

For the lower order plate/shell theories based on either Kirchhoff or Reissner hypothesis the through the thickness variation of inplane displacements $u_\alpha$ are linear, that is, $q = 1$ and $dim[S_{1D}^G(t = T, q)] = 2$, while the transverse displacement $u_3$ variation is constant, that is, $q = 0$ and $dim[S_{1D}^G(t = T, q)] = 1$.

To define the subspace in the local mesh which is to be constrained, $\hat{S}^L$ we limit ourselves to the case where the global space defined on the local region is a subspace of the local superimposed space, that is, $S^G(\Omega^L, p^G, q) \subset S^L(\Omega^L, p^L)$. In this scenario it is sufficient to constrain dofs of the local mesh corresponding to the following subspace:

$$\hat{S}^L = S^G_{1D} \otimes S^G_{2D} \tag{26}$$

This implies that it is necessary to constrain a number of shell surfaces or layer interfaces in the superimposed (DL) mesh equal to $dim[S^G_{1D}]$. In numerical examples we have constrained the top and bottom surfaces for inplane displacement and a bottom (or top) surface for the transverse displacement.

The second case of practical interest is that of partial superposition in the transverse direction as shown in Figure 1. This is especially important for multilayer composite with hundreds of layers, where it is desirable to superimpose only in the vicinity of most critical layers. In this scenario it is necessary to enlarge the constraint set $\hat{S}^L$ to maintain displacement compatibility between global and local meshes by constraining the dofs in the superimposed mesh at the global-local interface $\Gamma^{GL}$.

For the case of unstructured superposition ($S_u$-version) the redundant modes are eliminated during the solution phase as elucidated in [2]. In the current work only the structured mesh superposition methodology has been considered.

*REMARK:* The *s*-method can be utilized to hierarchically model discontinuous fields [3]. By this technique a mathematical model free of discontinuities is superimposed by an additional field able to represent the discontinuity. The mathematical validation of this technique was given in [3]. In the present study the global ESL mesh free of delamination is superimposed by a local 3D mesh with delamination (discontinuity) modeled by double nodes along the delamination surface. Numerical investigation is presented in section 5.

# 3. Assumed Strain formulation

To enhance the performance of the degenerated plate/shell elements primarily at lower spectral orders ($p \leq 4$) assumed strain formulation is employed. The formulation of the enhanced strain-displacement matrix $\bar{\mathbf{B}}$ can be obtained by interpolating $B_{ijA}$ between a set of reduced quadrature points [11] or by selectively projecting out higher order modes in the quadrature process as described in this section.

The formulation of assumed strain displacement matrix based on interpolating certain information between a set of reduced quadrature points is computationally taxing for higher order elements ($p > 4$), making the stiffness calculations cumbersome. To speed up this process Symmetric Dot Product(SDP) quadrature scheme (presented in [5]) which exploits the hierarchical structure of the stiffness matrix and eliminates the need for explicit strain interpolation between reduced and regular quadrature points has been developed in the context of the *s*-method. We briefly outline the SDP quadrature scheme in the context of laminated composites.

Consider the integral of the form $\int_\Omega g(\xi_1, \xi_2, \xi_3)\, h(\xi_1, \xi_2, \xi_3)\, d\Omega$ in the natural coordinate system such that $d\Omega = d\xi_1\, d\xi_2\, d\xi_3$ and $-1 \leq \xi_i \leq 1$. The integral under

consideration may represent a typical stiffness matrix component, where $g$ is a strain-displacement matrix component and $h$ is a strain-displacement matrix term multiplied by a jacobian and a corresponding component of the constitutive tensor. In the classical Gauss quadrature the integrand ($gh$) is implicitly curve fit with a polynomial and then integrated in a closed form. It has been shown in [8] that for hierarchical systems it is more efficient to curve fit separately each term of the integrand ($g$ and $h$) with orthonormal polynomials ($\phi$) which allows one to decompose the integral into a dot product of two vectors

$$\int_\Omega g\ h\ d\Omega = \sum_{I=1}^{L} \int_\Omega g\ \phi_I d\Omega \ \int_\Omega h\ \phi_I d\Omega \tag{27}$$

where the following concise notation is being used $\phi_I(\xi_1,\xi_2,\xi_3) \equiv \hat{P}_i(\xi_1)\hat{P}_j(\xi_2)\hat{P}_k(\xi_3)$ where $\hat{P}_i$ are normalized Legendre polynomials. $L = (l_1+1)(l_2+1)(l_3+1)$; where $l_i \ \ i \in [1,3]$ are polynomial orders of $\phi_I$ in $\xi_1,\xi_2,\xi_3$ directions, defined as in [5]. The proof is based on the orthogonality of Legendre polynomials and is given in [5] [8]. Now consider a typical stiffness term

$$k_{AB} = \int_\Omega \underbrace{\mathbf{B}_A^T\ \mathbf{D}\ \mathbf{B}_B\ J}_{\mathbf{g}_A\ \mathbf{h}_B}\ d\Omega \tag{28}$$

Let

$$\mathbf{g}_A\ =\ \mathbf{B}_A^T\ J^{1/2} \qquad \mathbf{h}_B\ =\ \mathbf{D}\ J^{1/2}\ \mathbf{B}_B \tag{29}$$

yielding

$$k_{AB} = \sum_{I=1}^{L} \int_\Omega \mathbf{B}_A^T\ J^{1/2}\ \phi_I d\Omega \ \int_\Omega \overbrace{\mathbf{D}\ \phi_I}^{\mathbf{g}_I} \underbrace{\mathbf{B}_B\ J^{1/2}}_{\mathbf{h}_B} d\Omega \tag{30}$$

and further dot product integral decomposition of the second term in (30) yields the following symmetric form:

$$k_{AB} = \sum_{I=1}^{L}\sum_{J=1}^{L} \int_\Omega \left(\mathbf{B}_A^T\ J^{1/2}\right)\ \phi_I d\Omega \cdot \underbrace{\int_\Omega (\mathbf{D})\ \phi_I\phi_J d\Omega}_{\mathbf{D}_{IJ}} \cdot \int_\Omega \left(\mathbf{B}_B^T\ J^{1/2}\right)\ \phi_J d\Omega \tag{31}$$

where the strain-displacement matrix $\mathbf{B}$ and the constitutive tensor are expressed in the element material coordinate system. For the exact integration of the term $\mathbf{B}_A^T\ J^{1/2}$ the maximum polynomial order of Legendre polynomial $\phi_I$ has to be equal to the maximum polynomial order of the integrand $\mathbf{B}_A^T\ J^{1/2}$. In practice the maximum polynomial order of $\phi_I$ is matched with the maximum polynomial order of $\mathbf{B}_A^T$ assuming a constant jacobian. Locking is alleviated by selectively projecting out the $\mathbf{B}$ matrix terms on to

a reduced space spanned by Legendre polynomials resulting in:

$$\int_\Omega \bar{\mathbf{B}}_A J^{1/2} \phi_I d\Omega = \int_\Omega \begin{bmatrix} b_{A11}\hat{\hat{P}}_i(\xi_1)\hat{P}_j(\xi_2)\hat{P}_k(\xi_3) \\ b_{A22}\hat{P}_i(\xi_1)\hat{\hat{P}}_j(\xi_2)\hat{P}_k(\xi_3) \\ b_{A33}\hat{P}_i(\xi_1)\hat{P}_j(\xi_2)\hat{\hat{P}}_k(\xi_3) \\ b_{A23}\hat{P}_i(\xi_1)\hat{\hat{P}}_j(\xi_2)\hat{\hat{P}}_k(\xi_3) \\ b_{A12}\hat{\hat{P}}_i(\xi_1)\hat{\hat{P}}_j(\xi_2)\hat{P}_k(\xi_3) \\ b_{A13}\hat{\hat{P}}_i(\xi_1)\hat{P}_j(\xi_2)\hat{\hat{P}}_k(\xi_3) \end{bmatrix} J^{1/2} d\Omega \tag{32}$$

where

$$\hat{\hat{P}}_m(\xi_t) = \begin{cases} \hat{P}_m(\xi_t) & m < l_t \\ 0 & m = l_t \end{cases} \tag{33}$$

Equation (33) is consistent with selective interpolation between reduced quadrature points [10] [11].

Note that if the constitutive tensor is constant, $\mathbf{D}_{IJ} = \int_\Omega \mathbf{D}\ \phi_I \phi_J d\Omega = \mathbf{D}\delta_{IJ}$. In case of Laminated Plates and Shells, $\mathbf{D}_{IJ}$ is pre-integrated.

# 4. Adaptive Strategy

Based on the information from *a posteriori* error estimators and indicators the adaptive procedure aims to achieve the the following objectives:

- Demarcation of critical regions where DL model should be superimposed.
- Polynomial refinement in both global(ESL) and local(DL) meshes until the desired level of accuracy is obtained.

The error indicators presented in this section are based on the earlier work by the authors [1]. The estimated error in the ESL model, referred as Dimensional Reduction Error (DRE), $\mathbf{E}$, is approximated by a linear combination of some basis functions $\phi$.

$$\mathbf{E} = \phi\, \beta \in E(\Omega^\star) \tag{34}$$

where $\beta$ are determined by solving the minimization auxiliary problem:

$$\frac{\partial}{\partial \beta}\{\frac{1}{2}a(\mathbf{u}^{FE} + \mathbf{E}, \mathbf{u}^{FE} + \mathbf{E})_\Omega - (\mathbf{u}^{FE} + \mathbf{E}, \mathbf{b})_\Omega - (\mathbf{u}^{FE} + \mathbf{E}, \mathbf{t})_\Gamma\} = 0 \tag{35}$$

and the functional space $E$ is defined to maintain $C^0$ continuity of the augmented field $\mathbf{u}^{FE} + \mathbf{E}$ and to satisfy essential boundary conditions, that is

$$E = \{\mathbf{E} | \mathbf{E} = \phi\beta \in C^0(\Omega^\star);\ \ \mathbf{E} \in S^E(\Omega^\star, p^E);\ \ \mathbf{E} = 0\ \ on\ \ \Omega \backslash \Omega^\star\} \tag{36}$$

We now define the subspace $S^E$. For the process of identification of critical regions in the ESL plate/shell model the $\mathbf{u}^{FE}$ corresponds a given ESL finite element solution and $\phi$ represents layer-wise 3D finite element interpolants. To estimate the dimensional reduction error indicators, the space $S^E$ is chosen as a 3D discrete layer interpolation

space defined on the entire domain $\Omega^\star = \Omega$, with maximum polynomial order $p^E = 1$. It is desirable that the computational effort of the error estimation process be only a fraction of the finite element solution, hence in practice only an approximation for $\beta$ is calculated. We will be seeking for an approximation of $\beta$ by replacing the Hessian matrix $a(\phi, \phi)$ resulting from (35) by its diagonal. The resulting energy norm of the estimated error for each element is obtained by:

$$\eta_e = \sum_{A}^{NDOFS} \{\frac{1}{2}\beta_A^2 a(\phi_A,\ \phi_A)_{\Omega^e}\}^{\frac{1}{2}} \tag{37}$$

where NDOFS are the total number of degrees of freedom in the element '$e$'. The critical elements which need to be superimposed are selected such that:

$$\eta_e \geq \gamma_e \max_e(\eta_e) \tag{38}$$

where parameter $\gamma_e \in [0, 1]$ controls the number of elements to be superimposed with $\gamma = 0$ corresponding to uniform superposition over the entire domain.

We now consider adaptive strategy based on selective polynomial escalation in the two meshes. Consider a given finite element space consisting of underlying and superimposed meshes

$$S^{FE} = S^G((\Omega^G \backslash \Omega^L), p^G, q, l^G) \cup [S^L(\Omega^L, p^L, l^L) \backslash \hat{S}^L(\Omega^L)] \tag{39}$$

and let us define a higher order space $S^E$ obtained by increasing the polynomial order of both global and local interpolants.

$$S^E = [S^G((\Omega^G \backslash \Omega^L), p^G + 1, q) \cup S^L(\Omega^L, p^L + 1) \backslash \hat{S}^L(\Omega^L)] \setminus S^{FE} = SPAN\{\phi_A\} \tag{40}$$

As before approximation for $\beta$ are found by replacing the Hessian matrix $a(\phi, \phi)$ by its diagonal. Error indicators corresponding to each higher order degree of freedom are calculated as:

$$\eta_A = \{\frac{1}{2}\beta_A^2 a(\phi_A,\ \phi_A)\}^{\frac{1}{2}} \quad \text{no sum on A} \tag{41}$$

in both meshes. The degree-wise error indicators $\eta_A$ is used in selection of critical basis functions which reduce the error similar to the element-wise error indicators(38). The list of active degrees of freedom $l^G$ and $l^L$ is appended with those degrees-of-freedom which correspond to the error indicators $\eta_A$ (41) such that:

$$\eta_A \geq \gamma \max_A(\eta_A) \tag{42}$$

where parameter $\gamma \in [0, 1]$ controls the speed of convergence with $\gamma = 0$ corresponding to uniform polynomial escalation.

# 5. Multigrid method for hierarchical systems.

The structure of the stiffness matrix resulting from the $s$-method is quite dense unlike the banded structure of the lower order elements. This is due to use of higher order

elements and explicit coupling between global and local meshes. The deterioration of the sparsity significantly affects the total solution time in the case of conventional sky-line or sparse matrix equation solvers. On the other hand, the hierarchical structure of $s$-method has a positive effect on the system conditioning. This suggests that iterative equation solvers are ideal to expedite the solution process. In our previous work [5] we have developed efficient Multigrid-like iterative solvers for $p$-method. These solvers are generalized to deal with positive definite systems arising from the superposition of ESL and DL meshes. We consider a hierarchical system:

$$\mathbf{K}^m \ \mathbf{d}^m \ = \ \mathbf{f}^m; \ \ m = \underbrace{0, 1, 2 \ldots m^G}_{global\ levels}, \overbrace{m^G + 1, \ldots m^G + m^L}^{local\ levels} \tag{43}$$

where

$$\mathbf{K}^m = \begin{bmatrix} \hat{\mathbf{K}}^{m-1} & \mathbf{K}^m_{12} \\ \mathbf{K}^m_{21} & \mathbf{K}^m_{11} \end{bmatrix} \quad \mathbf{d}^m = \begin{Bmatrix} \mathbf{d}^{m-1} \\ \mathbf{d}^m_1 \end{Bmatrix} \quad \mathbf{f}^m = \begin{Bmatrix} \mathbf{f}^{m-1} \\ \mathbf{f}^m_1 \end{Bmatrix} \tag{44}$$

and $m$ is the level number; $\mathbf{K}^0$ the stiffness matrix on the initial level; $\mathbf{K}^m$ is of order $n_m > n_{m-1}$, where $n_{m-1}$ is the order of the block $\hat{\mathbf{K}}^{m-1}$; $\mathbf{d}^m_1 \in \Re^{(n_m - n_{m-1})}$ and $\mathbf{d}^{m-1} \in \Re^{n_{m-1}}$.

The special feature of the equation (44) for superposition analysis is that lower order block $\hat{\mathbf{K}}^{m-1}$ might be different from the stiffness matrix corresponding to level $(m-1)$, $\mathbf{K}^{m-1}$, because of either

1. Change in constitutive model from plane stress ($q = 1$) to 3-D ($q \geq 2$).
2. Progressive improvement in geometry or
3. Changing quadrature scheme.

The global plate/shell model may exhibit somewhat stiffer behavior at lower polynomial orders which may not well represent a lower frequency response of the total superimposed system. This is related to well known problem of "locking" which is characteristic of lower order plates and shells.

We now present a variant of the multigrid method for solving positive definite systems defined by equation (44). Let $\mathbf{Q}^{m-1}_m$ and $\mathbf{Q}^m_{m-1}$ be the restriction and prolongation operators, which transfer the data from level $(m)$ to level $(m-1)$ and vice versa. Due to hierarchiality of the $s$-method it has a very simple form:

$$\mathbf{Q}^{m-1}_m \ = \ [\mathbf{I} \ \ \mathbf{0}] \ = \ {\mathbf{Q}^m_{m-1}}^T \tag{45}$$

where $\mathbf{I}$ is the order $n_{m-1}$ identity matrix, and $\mathbf{0}$ is order $(n_m - n_{m-1})$ zero matrix. A single V-cycle has a compact recursive definition given by:

$$\mathbf{z}^m := MG^m(\mathbf{r}^m, \mathbf{K}^m). \tag{46}$$

where $\mathbf{r}^m$ is the residual vector. The V-cycle multigrid algorithm is summarized below:

1. Loop $i = 0, 1, 2 \ldots$ until convergence
   if $i \ = \ 0 \ \leftarrow \ \mathbf{d}^m \ = \ 0$

2. perform $\gamma_1$ pre-smoothing operations

$$_{\gamma_1}{}^{i}\mathbf{d}^m := \text{smooth}(\gamma_1, {}_0{}^{i}\mathbf{d}^m, \mathbf{K}^m, \mathbf{f}^m)$$

where the left superscript and subscript denote the cycle number and smoothing count respectively.

3. Restrict residual from level $m$ to $m-1$

$$\mathbf{r}^{m-1} = \mathbf{Q}_m^{m-1}(\mathbf{f}^m - \mathbf{K}^m {}_{\gamma_1}{}^{i}\mathbf{d}^m)$$

4. Coarse grid correction
   If $(m-1)$ = lowest level, solve directly $\mathbf{z}^{m-1} = (\mathbf{K}^{m-1})^{-1}\mathbf{r}^{m-1}$,
   Else $\mathbf{z}^{m-1} := MG^{m-1}(\mathbf{r}^{m-1}, \mathbf{K}^{m-1})$

5. Prolongate from level $m-1$ to $m$

$$_{\gamma_1+1}{}^{i}\mathbf{d}^m = {}_{\gamma_1}{}^{i}\mathbf{d}^m + {}^{i}\omega\, \mathbf{Q}_{m-1}^m \mathbf{z}^{m-1}$$

where ${}^{i}\omega$ is a coarse grid relaxation parameter, which minimizes energy functional along the prescribed direction $\mathbf{v}^m = \mathbf{Q}_{m-1}^m \mathbf{z}^{m-1}$ and is given as:

$${}^{i}\omega = \frac{\mathbf{v}^{mT}(\mathbf{f}^m - \mathbf{K}^m {}_{\gamma_1+1}{}^{i}\mathbf{d}^m)}{\mathbf{v}^{mT}\,\mathbf{K}^m\,\mathbf{v}^m} \tag{47}$$

Note that for two grid methods ${}^{i}\omega = 1$ if $\hat{\mathbf{K}}^{m-1} = \mathbf{K}^{m-1}$.

6. Perform $\gamma_2$ post-smoothing operations

$$^{i+1}{}_0\mathbf{d}^m := \text{smooth}(\gamma_2, {}_{\gamma_1+1}{}^{i}\mathbf{d}^m, \mathbf{K}^m, \mathbf{f}^m)$$

Another variant of the standard V-cycle multigrid method [18] has been proposed by Bank, Dupont and Yserentant [12]. The method termed as hierarchical basis multigrid technique(HBM), is similar to the standard multigrid V-cycle, except that a smaller than the normal subset of unknowns is updated during the smoothing phase at a given level. HBM takes advantage of the fact that smoothing mainly affects highest oscillatory modes of error, and thus relaxation sweeps are performed on the block by block level keeping the rest of the degrees of freedom fixed. It has been shown by Bank, Dupont and Yserentant(1988) that the rate of convergence of HBM method has a logarithmic dependence on the problem size as opposed to multigrid method which has an optimal rate of convergence independent of the mesh size and spectral order.

For ill-conditioned problems, such as thin laminated plates and shells, it is desirable to accelerate the rate of convergence of the multigrid like methods. The acceleration schemes (Two parameter and Conjugate Gradients) require a small fraction of computational effort, but at the same time have been found to be very efficient in expediting the convergence of the multigrid like methods[5].

# 6. Numerical Experiments

Numerical experiments are conducted to investigate the performance of $s$-method for modeling laminated composites in terms of accuracy and computational efficiency. The following classical test problems are considered:

- $(45/-45)_s$ laminate in axial tension [27][30][26]
- $(45/0/-45/90)_s$ laminate in axial tension [27]
- Edge delamination test for $(0/35/-35/90)_s$ laminate[26]
- Composite laminate Scordelis-lo roof.

Geometry, boundary conditions and material properties for the axial tension problems are illustrated in Fig. 2 and 3.

Our numerical experimentation agenda involves investigation of the following aspects:

- Ability of Dimensional Reduction Errors to capture critical regions.
- The influence of mesh gradation, selective polynomial escalation and assumed strain formulation on the rate of convergence.
- Comparative study of iterative and direct solution techniques for laminated composites.

Contour lines of the estimated error for $(45/-45)_s$ and $(45/0/-45/90)_s$ laminates subjected to axial tension are given in Fig. 2 and 3 respectively. The contour lines were obtained by interpolating estimated elemental errors. The estimated error distribution substantiates the well known fact that edge effects are prominent near the free edges of the laminates. A layer-wise finite element mesh is superimposed over the critical elements.

In our current study identical inplane mesh subdivision for underlying and overlying meshes has been employed. Numerical comparison of meshes with different gradation in resolving 3D stress fields in $(45/-45)_s$ laminate is illustrated in Fig. 5. The uniform superimposed mesh shown in Fig. 4 is obtained by layer-wise subdivision in the transverse direction. The two geometric meshes in Fig. 4 have layers of elements graded towards the free edge and the ply interface with a common factor of 0.15. Normalized stress distribution ($\bar{\sigma_{i3}} = \sigma_{i3}/\epsilon_0$ where $\epsilon_0$ = axial strain) near the free edges for each type of mesh is shown in Fig. 5. The reference stress distributions at the free edges are depicted from [30],[26][27]. It is evident from the plots in Fig. 5 that geometric meshes are vital to accurately estimate the stress field near free edges and polynomial order escalation alone in uniform meshes is not sufficient.

Assumed strain and displacement based elements (for both underlying and superimposed models) as well as the quadrature schemes are compared in Fig. 6. The CPU times required for the calculation of total (global and local) stiffness employing SDP and uniform quadrature schemes are compared for the $(45/-45)_s$ problem modeled with two level geometric mesh (Fig. 4). Plots of absolute maximum stress and error in energy norm versus the total CPU time for stiffness calculation are shown in Fig. 6. Both formulations are quite competent in estimating maximum stresses, although the

assumed strain formulation has faster convergence. Moreover it is evident that SDP quadrature is computationally more efficient than the uniform quadrature scheme for both assumed strain and displacement based elements.

To study the effect of selective polynomial order escalation on the resolution of free edge stresses, the $(45/-45)_s$ and $(45/0/-45/90)_s$ laminates modeled with meshes as shown in Fig. 7 and 8 respectively, are considered. In Fig. 7 and 8 plots of maximum stresses with and without selective polynomial order escalation for the local mesh are presented for $(45/-45)_s$ and $(45/0/-45/90)_s$ laminates. It is evident that selective polynomial order escalation speeds up the rate of convergence. In the problems considered the parameter $\gamma$ (42) was set equal to 0.01 and selective polynomial order escalation was performed only on the local mesh.

In Fig. 9 the composite laminate Scordelis-lo roof problem is investigated. The elemental error densities in a 4x4 uniform mesh are illustrated. The two elements with maximum errors are superimposed with discrete layer mesh. The parameter $\gamma_e$ was chosen as 0.75. The convergence in energy norm and in the maximum normal stress with uniform and selective polynomial escalation are depicted in the plots. Selective polynomial escalation is carried out in both local and global meshes. It is evident from the plots that selective polynomial escalation simultaneously in both meshes has to be carried out, selective polynomial escalation in the local mesh alone is not sufficient unless the global mesh is sufficiently refined.

Partial through-the-thickness mesh superposition where only two (0,-45) lamina are superimposed in the $(45/0/-45/90)_s$ laminate, is presented in Fig. 10. It can be seen that the accuracy of stresses at the (0/-45) interface is not significantly compromised due to the partial superposition.

The edge delamination tension (EDT) problem is used to test the ability of the model to predict energy release rates. The particular laminate chosen for this experiment is $(0/35/-35/90)_s$, since this problem has been analyzed using layer-wise theory in [26] and using quasi-3D finite element model in [28]. The geometry, boundary conditions, symmetry and material properties are illustrated in Fig. 11. The specimen has four delaminations two along each free edge at the $-35/90$ and $90/-35$ interfaces. The delamination surface interpenetration has been ignored in the current study. Three dimensional Virtual crack closure method [29] is used to calculate the total energy release rate and its components. In Fig. 11 normalized energy release rates are plotted versus the specimen length. The energy release rates are normalized as follows:

$$(\bar{G},\, \bar{G}_I,\, \bar{G}_{II}) = \frac{(G,\, G_I,\, G_{II})}{\epsilon_0^2\; 0.5t\; L} \tag{48}$$

where $L$ is the length of the specimen, $t$ the total thickness and $\epsilon_0$ the uniform axial strain. It was observed that the contribution of mode III towards the total energy release rate was negligible and mode II was the prominent contributor. The energy release rates are fairly constant along the central portion of the specimen and show a decrease near the ends, where the delamination surfaces are constrained against relative motion to simulate friction grips. The results presented match closely with the results presented in [26] in the central portion of the specimen.

Finally we study the performance of various solution techniques for solving a positive definite linear system of equations resulting from $s$-version of finite element for-

mulation. The $(45/0/-45/90)_s$ laminate problem (Fig. 8) and the Scordelis-lo roof problem have been considered. The solution procedures considered are :

- MG-ICC-ACC:: Multigrid method with In-Complete Cholesky smoothing and two parameter acceleration.
- HBM-ICC-ACC:: Hierarchical Basis Multigrid method with In-Complete Cholesky smoothing and two parameter acceleration.
- PCG-ICC:: Pre-conditioned Conjugate Gradient Method with In-Complete Cholesky Preconditioner.
- Direct:: LDU skyline solver.
- Sparse Direct:: The sparse direct solver developed by NASA [31].

It is evident from the plot of number of degrees-of-freedom versus CPU time required for solution in Fig. 12 that the Multigrid-like solvers have better performance for larger well conditioned systems (number of dofs $> 2000$) than the sparse direct solver. Amongst the MG-like solvers HBM is computationally more efficient because Incomplete Cholesky factorization of the block diagonal matrix (used for HBM-ICC smoothing) is relatively inexpensive compared to that of the entire dense matrix used for MG-ICC smoothing. For the Scordelis-lo roof problem the breakeven problem size between iterative and direct solvers moves upwards, because of poor conditioning of the stiffness matrix. The Incomplete Cholesky smoothing has been found to be superior than the Gauss Seidel smoothing in particular for poor conditioned thin domain problems. All the experiments were conducted on a Sun Sparc 10 workstation.

# References


[1] J. Fish, S. Markolefas, R. Guttal, and P. Nayak, "On adaptive multilevel superposition of finite element meshes for linear elastostatics." *Appl. Numer. Math.*, 14, 135-164(1994).

[2] J. Fish, "The *s*-version of the finite element method", SCOREC report #18-1990, Rensselaer Polytechnic Institute Troy, NY-12180; and *Comput. and Struct.*, 43, 539-547(1990)

[3] J. Fish, "Hierarchical modeling of discontinuous fields." Comm. Appl. Numer. Methods, 8, 443-453 (1992).

[4] J. Fish and S. Markolefas, "The *s*-version of the finite element method for multilayer laminates" *Int. J. Numer. Methods Eng.*, 33, 1081-1105(1992).

[5] J. Fish and R. Guttal, "The *p*-version of Finite Element Method for Shell Analysis." *Comp. Mech. Int. Journal*, 16, 1-13(1995).

[6] J. Fish and S. Markolefas, "Adaptive global-local refinement strategy based on interior error estimates of the *h*-method." *Int. J. Numer. Methods Eng.*, 37, 828-838, (1994).

[7] I. Babuska, S. Stroubulis, C. S. Upadhyay and S. K. Gangaraj, "A posteriori estimation and adaptive control of the polluting error in the $h$-version of the finite element method." Technical note BN-1175, Institute for Physical Science and Technology, Univ. of Maryland, College Park, MD.

[8] H. Hinnant, "A Fast method of numerical quadrature for $p$-version finite element matrices", *A.I.A.A.*, 1386(1993).

[9] B. A. Szabo and I. Babuska, "Finite element Analysis." Wiley. (1991).

[10] K. C. Park, G. M. Stanley, "A curved $C^0$ Shell element based on Assumed Natural Coordinate Strains." *J. of Appl. Mech.*, 108, 278-290(1986).

[11] T. J. R. Hughes, "The Finite Element Method." Prentice-Hall. (1987).

[12] R. E. Bank, T. F. Dupont and H. Yserentant, "The hierarchical basis multigrid method." *Numer. Math.*, 52, 427-458 (1988).

[13] S. F. McCormick and J. W. Thomas, "The fast adaptive composite grid (FAC) method for elliptic equations." *Mathematics of Comput.*, 46, 439-456, (1986).

[14] J. Bramble, R. E. Ewing, J. E. Pasciak and A. H. Schatz, "A preconditioning technique for the efficient solution of problems with local grid refinement." *Comp. Meth. Appl. Mech. Eng.*, 67, 149-159 (1988).

[15] J. E. Flaherty, P. K. Moore and C. Ozturan, "Adaptive overlapping methods for parabolic systems." in Adaptive Methods for Partial Differential Equations (Eds. J. E. Flaherty, P. J. Paslow, M. S. Shephard and J. D. Vasilakis), SIAM (1989).

[16] J. D. Whitcomb, "Iterative global-local finite element analysis." *Computers and structures,* 40, 1027-1031 (1991).

[17] J. Fish and V. Belsky, "Mutligrid method for periodic heterogeneous media. Part 2: Multiscale modeling and quality control in multidimensional case." accepted in *Comp. Meth. Appl. Mech. Eng.*,(1994).

[18] A. Brandt, "Multi-level adaptive solutions to boundary-value problems." *Mathematics of Computation,* 31, 333-390 (1977).

[19] T. Belytschko, J. Fish and A. Bayliss, "The spectral overlay on finite elements for problems with high gradients." *Comp. Meth. Appl. Mech. Eng.*, 81, 71-89 (1990).

[20] H. Yserentant, "On multilevel splitting of finite element spaces." *Numer. Math.*, 379-412, (1986).

[21] J. N. Reddy and D. H. Robbins, "Theories and computational models for composite laminates." *Appl. Mech. Rev.*, 47, 147-169 (1994).

[22] A. K. Noor, W. S. Burton and J. M. Peters, "Predictor-Corrector procedures for stress and free vibration analyses of multilayered composite plates and shells." *Comp. Meth. Appl. Mech. Eng.*, 82, 341-363, (1990).

[23] N. F. Knight, J. B. Ransom, O. H. Griffin and D. M. Thompson, "Global/Local methods research using a common structural analysis framework." *Finite Element Analysis and Design,* 9, 91-112 (1991).

[24] K. M. Mao and C. T. Sun, " A refined global-local finite element analysis method." *Int. J. Numer. Methods Eng.*, 32, 29-43 (1991).

[25] J. Fish, V. Belsky and M. Pandheeradi, "Composite grid method for hybrid systems." submitted to *Comp. Meth. Appl. Mech. Eng.*, (1995).

[26] D. H. Robbins, Y. S. N. Reddy and J. N. Reddy, "Analysis of Inter-laminar Stresses and Failures using a Layer-Wise Laminate Theory, Local Mechanics Concepts For Composite Material Systems". Springer-Verlag, Eds. J.N. Reddy and K.L. Reifsnider, 309-340 (1991).

[27] J. D. Whitcomb, I. S. Raju and J. G. Goree "Reliability of the Finite Element Method for calculating Free edge stresses in composite laminates." *Computers and structures,* 15, 23-27 (1982).

[28] I. S. Raju, J. H. Crews.Jr. and M. A.Aminpour, "Convergence of Strain Energy release rate components for Edge-Delaminated Composite Laminates." NASA Technical Memorandum 86135 (1987).

[29] K. N. Shivakumar, P. W. Tan and J. C. Newman, "A Virtual Crack Closure Technique for Calculating Stress-Intensity factors for Cracked Three-dimensional Bodies." *Int. J. of Fracture,* 36, R43-R50 (1988).

[30] S. S. Wang and I. Choi, "Boundary-Layer Effects in Composite Laminates: Part 2-Free-Edge Stress Solutions and Basic Characteristics". *J. of Appl. Mech,* 49, 549-560 (1982).

[31] Olaf. Storaasli, NASA. LaRC. Hampton VA. 23681.

# MESH SUPERPOSITION ON LAMINATED SHELL

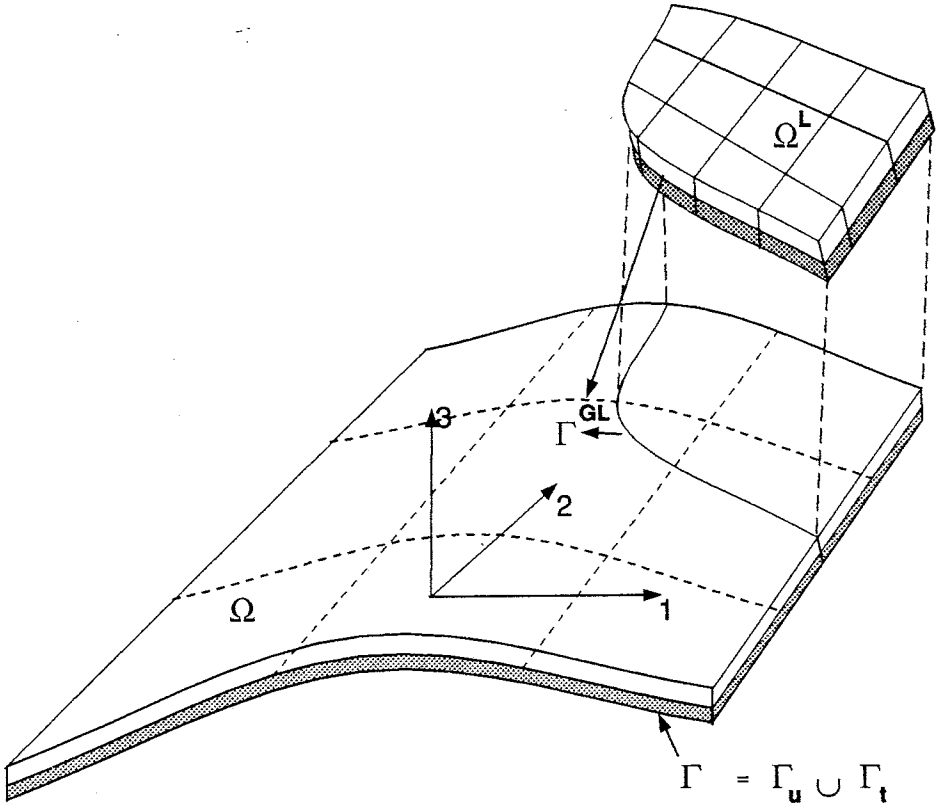


**PARTIAL SUPERPOSITION**

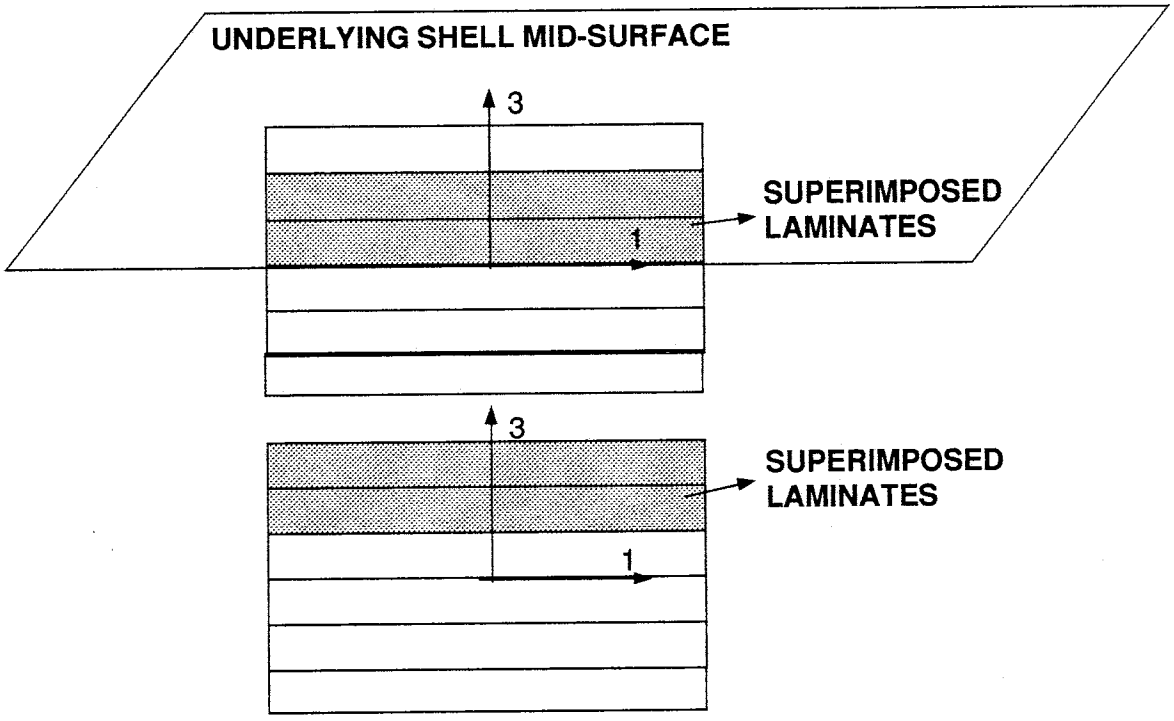


**Figure 1.**

# AXIAL TENSION (45/-45) PROBLEM

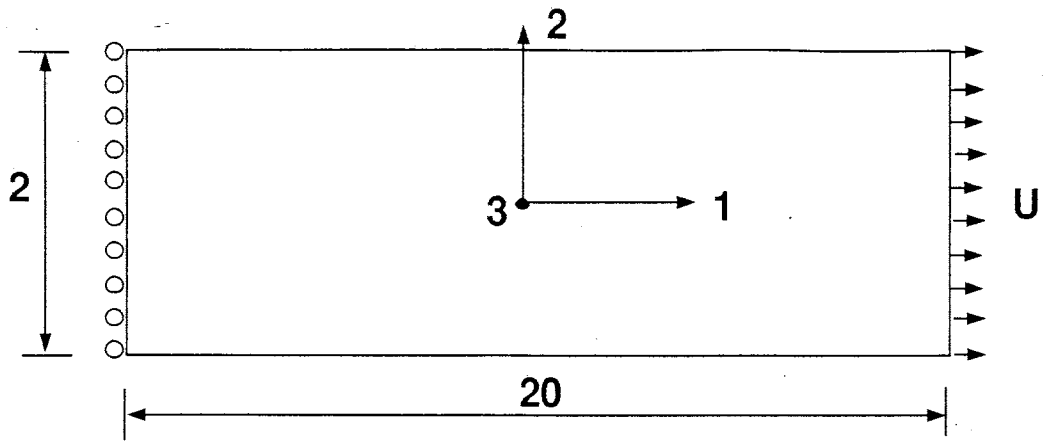


**Thickness of each lamina = 0.125**

$E_1 = 20.0 \times 10^6$ psi,

$E_2 = E_3 = 2.10 \times 10^6$ psi

$G_{12} = G_{23} = G_{13} = 0.85 \times 10^6$ psi,

$\nu_{12} = \nu_{23} = \nu_{13} = 0.21.$

FIGURES NOT TO SCALE

## D.R.E. INDICATOR CONTOURS AT 45/-45 INTERFACE

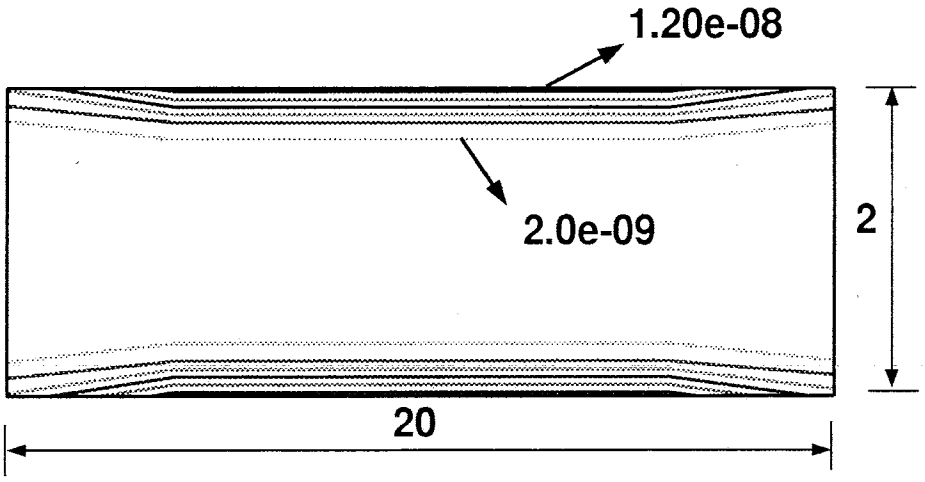


Figure 2.

# AXIAL TENSION PROBELM (90/-45/0/45)s COMPOSITE LAMINATE

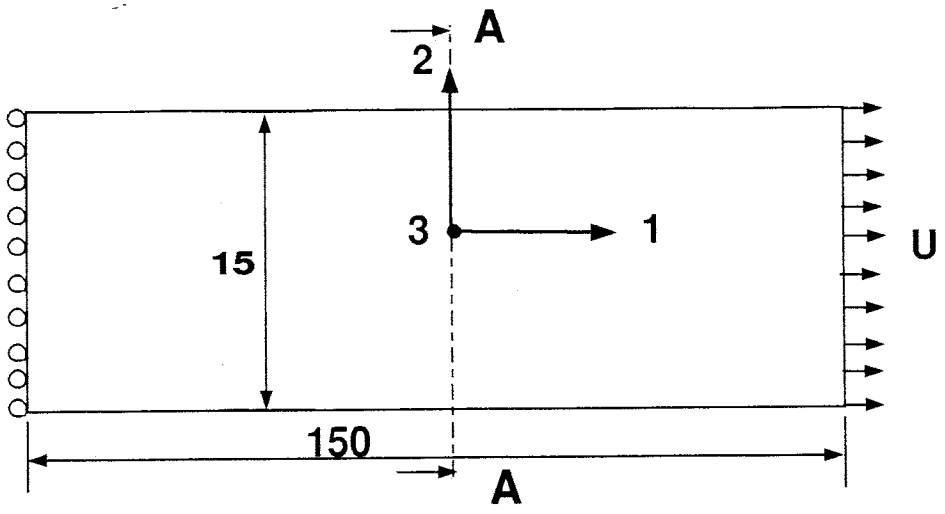


**Thickness of each lamina = 0.125**

$E_1 = 19.5 \times 10^6$ psi,

$E_2 = E_3 = 1.48 \times 10^6$ psi

$G_{12} = G_{23} = G_{13} = 0.8 \times 10^6$ psi,

$\nu_{12} = \nu_{23} = \nu_{13} = 0.30.$

FIGURES NOT TO SCALE

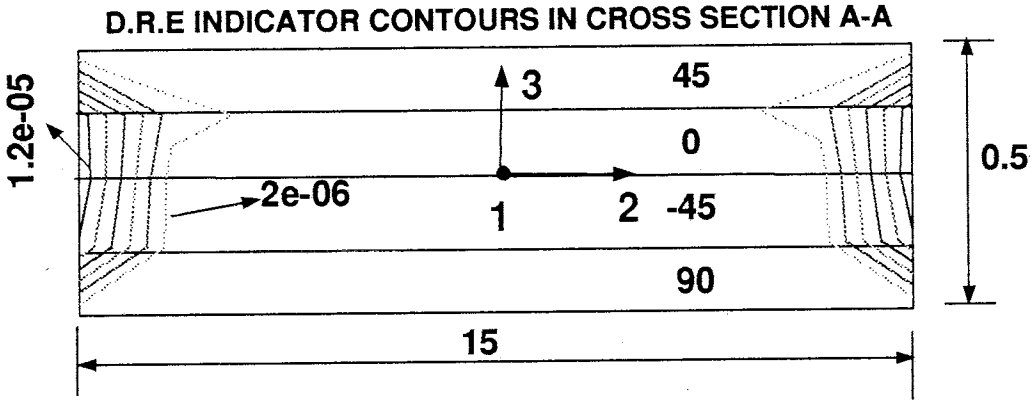


Figure 3

# DIFFERENT MESHES USED FOR FREE EDGE STRESS ESTIMATION

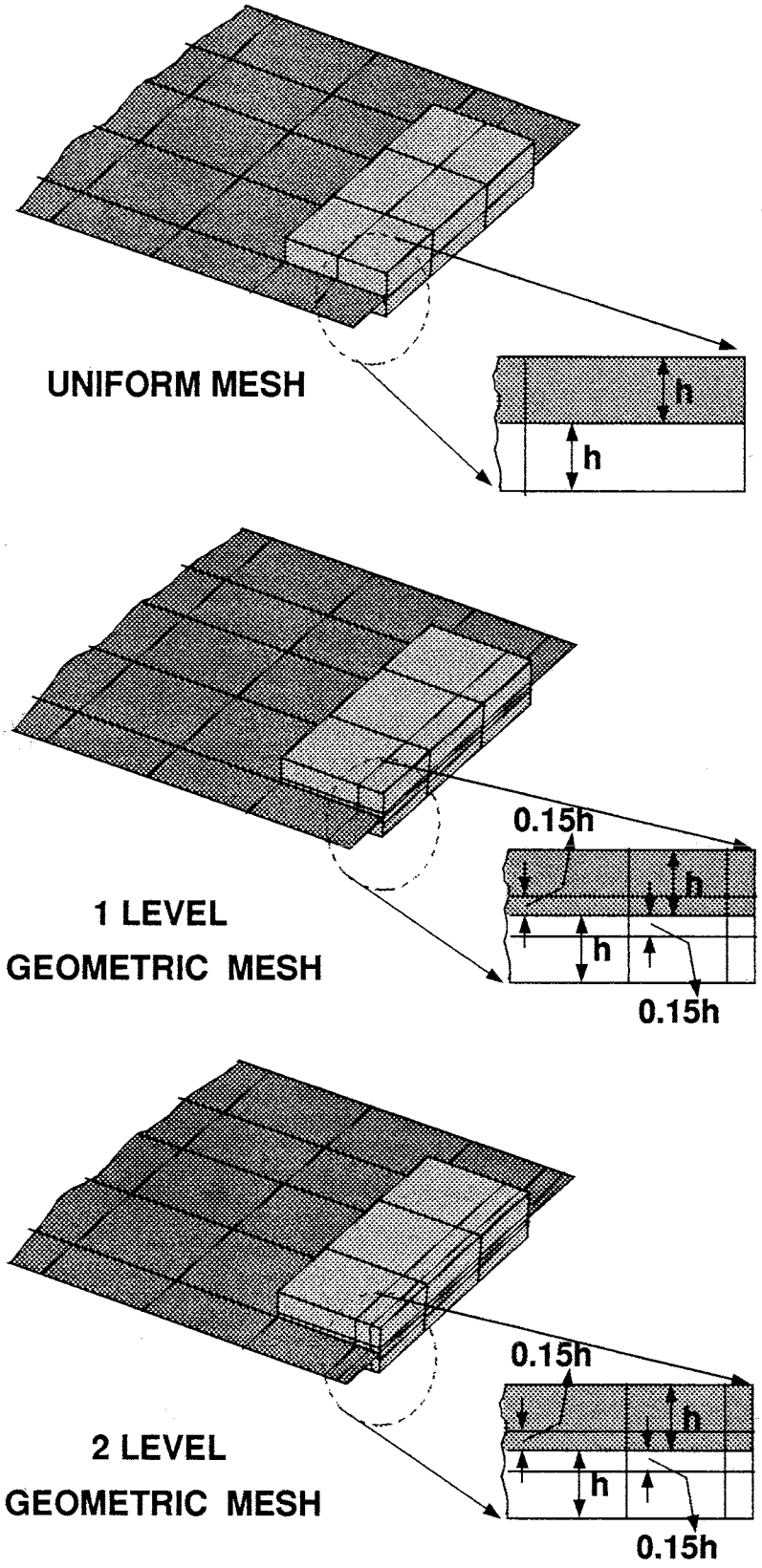


Figure 4

## COMPARISON OF MESHES FOR (45/-45)s LAMINATE

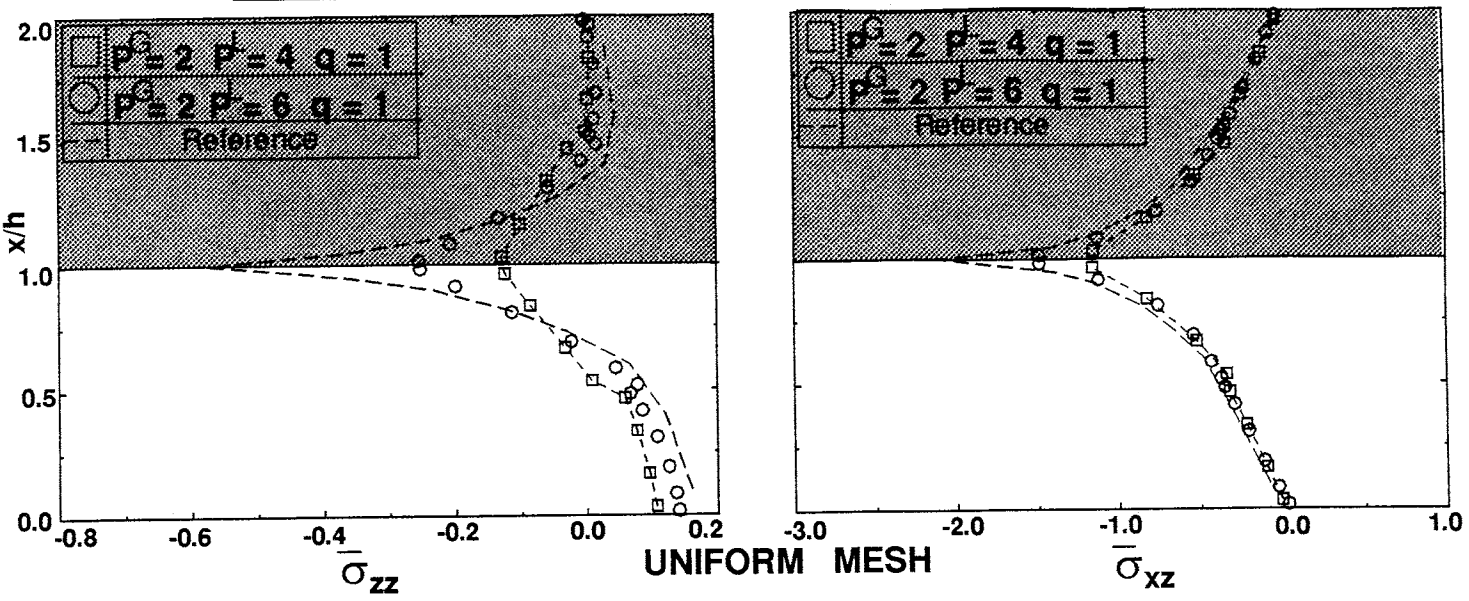


UNIFORM MESH

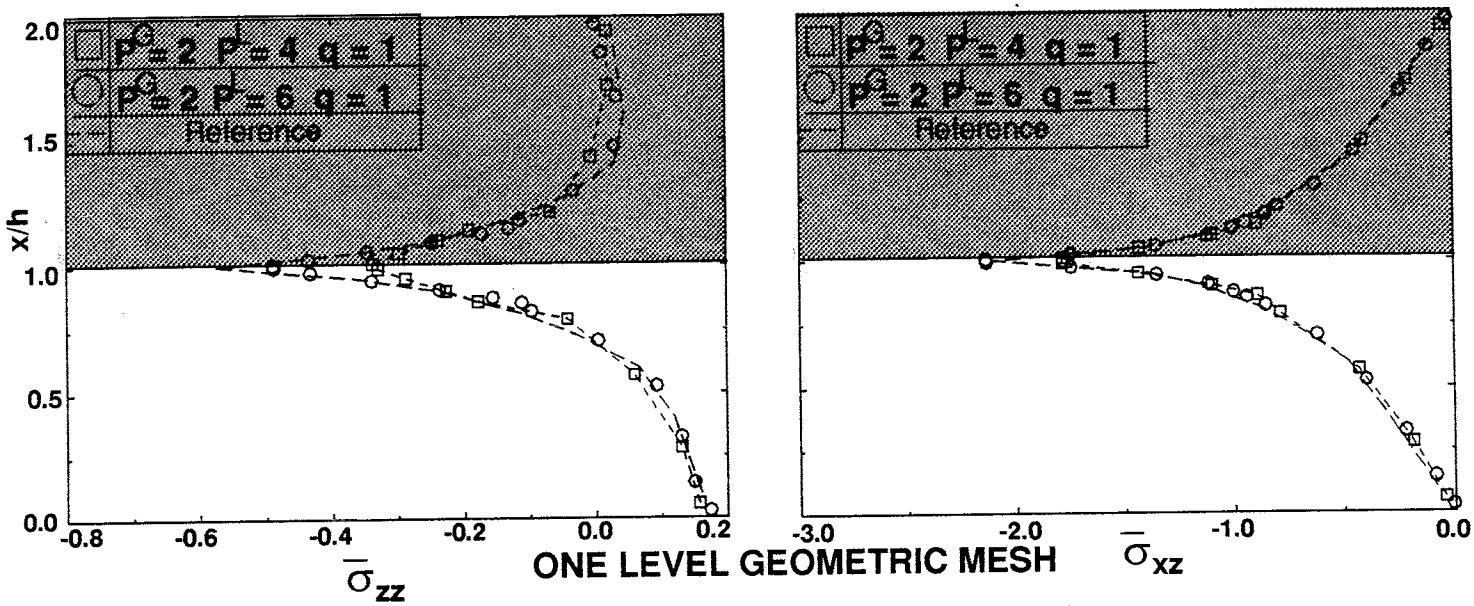


ONE LEVEL GEOMETRIC MESH

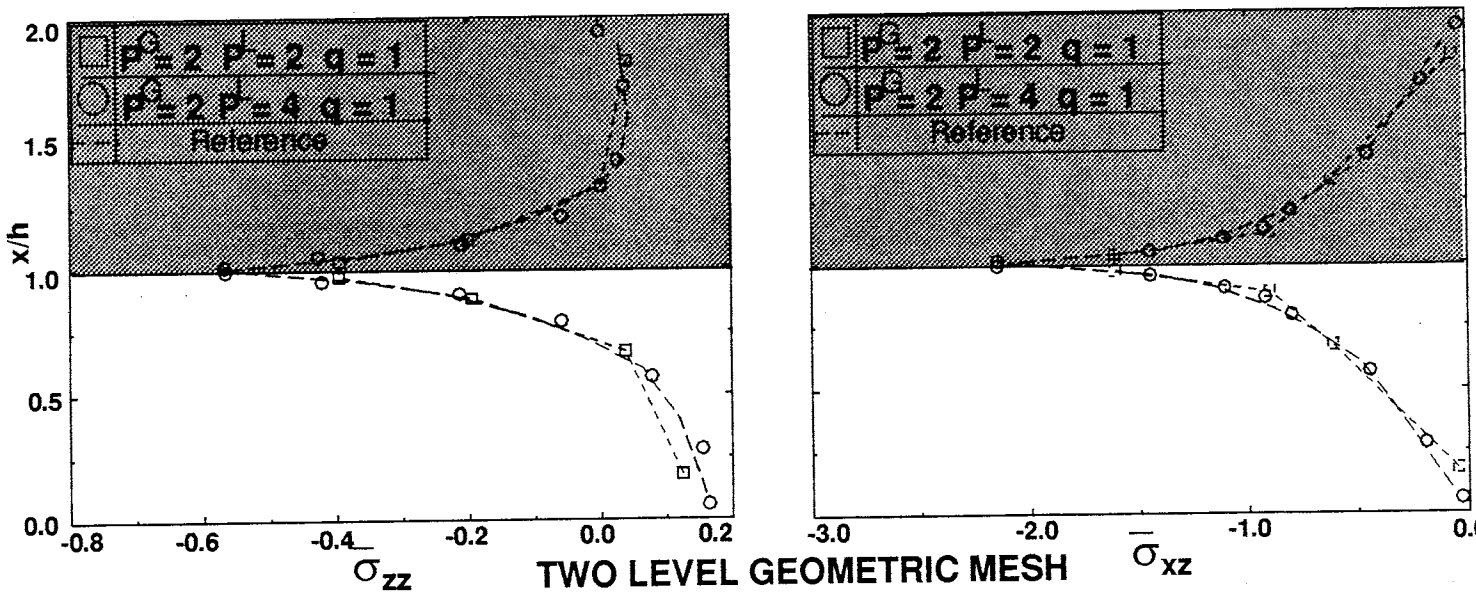


TWO LEVEL GEOMETRIC MESH

Figure 5.

## COMPARISON OF QUADRATURE SCHEMES

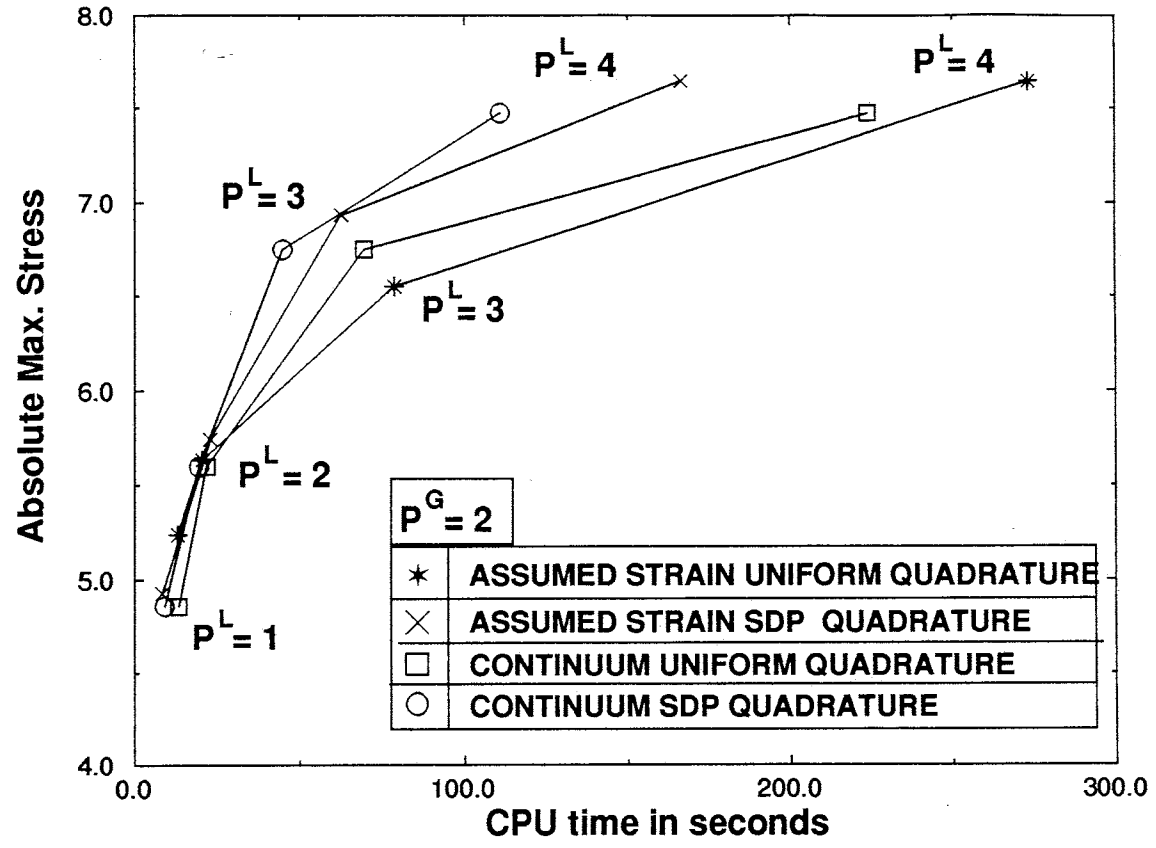


## TWO LEVEL GEOMETRIC MESH (45/-45)s LAMINATE

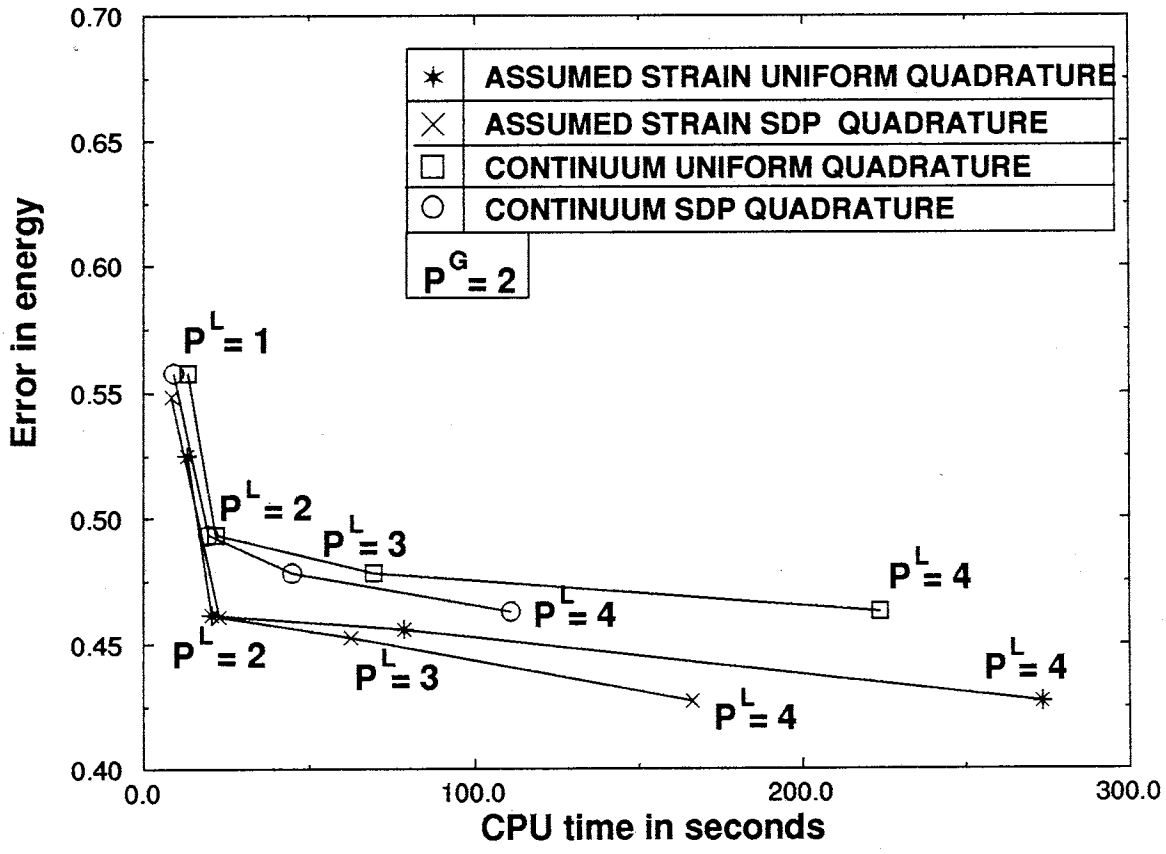


Figure 6

# EFFECT OF SELECTIVE REFINEMENT (45/-45)s LAMINATE

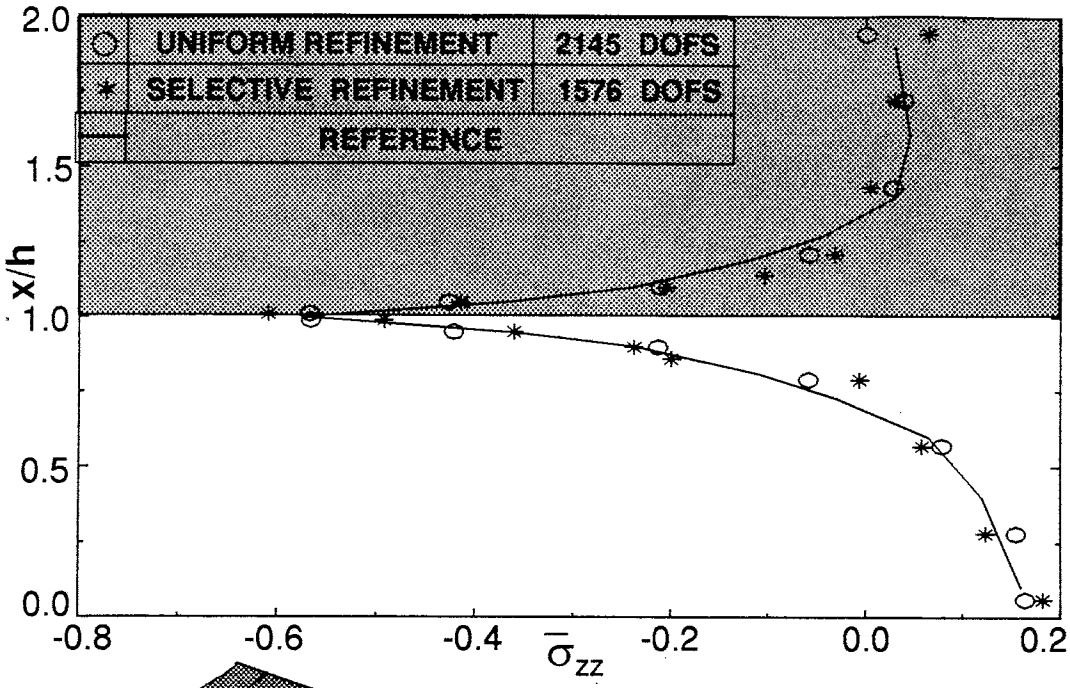


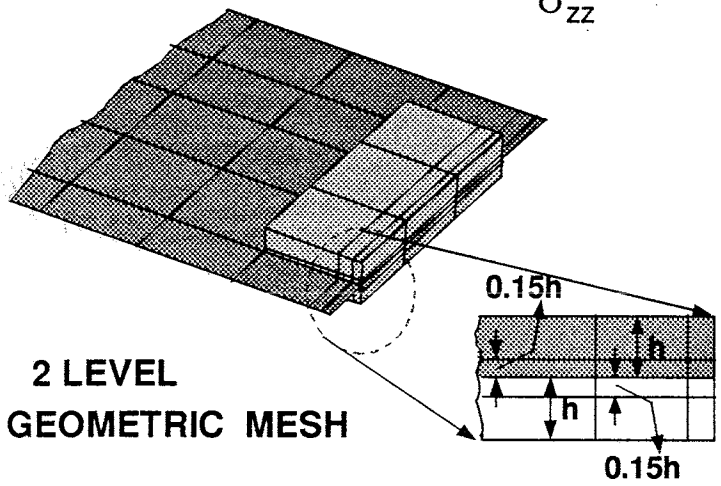


2 LEVEL
GEOMETRIC MESH

GLOBAL POLYNOMIAL ORDER = 2
LOCAL POLYNOMIAL ORDER = 4

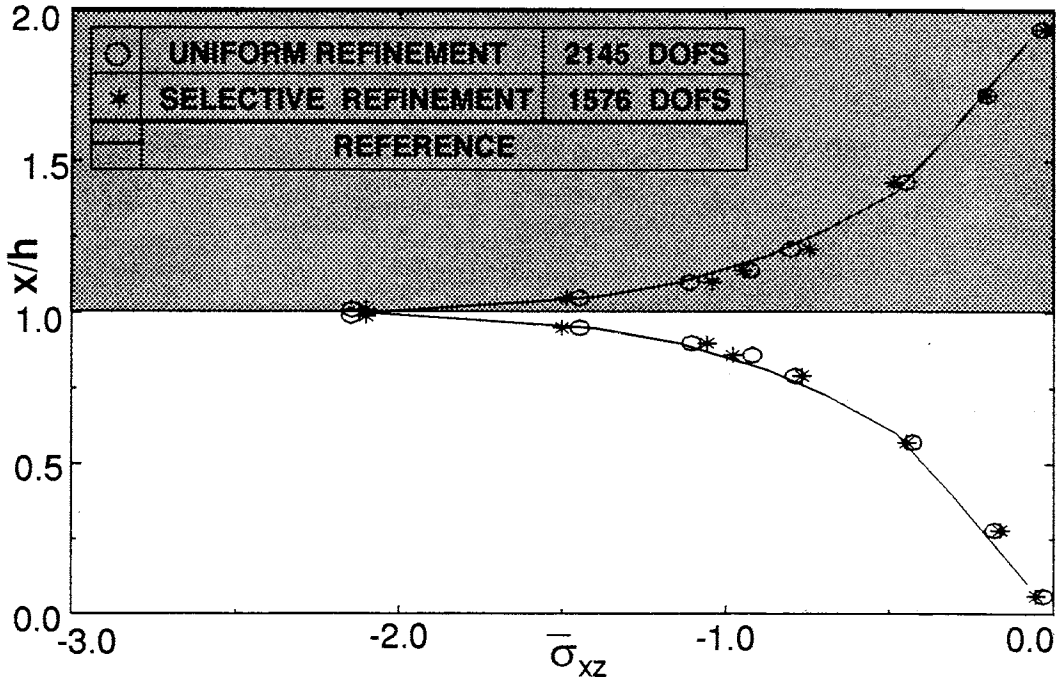


Figure 7.

## EFFECT OF SELECTIVE REFINEMENT (45/0/-45/90)s LAMINATE

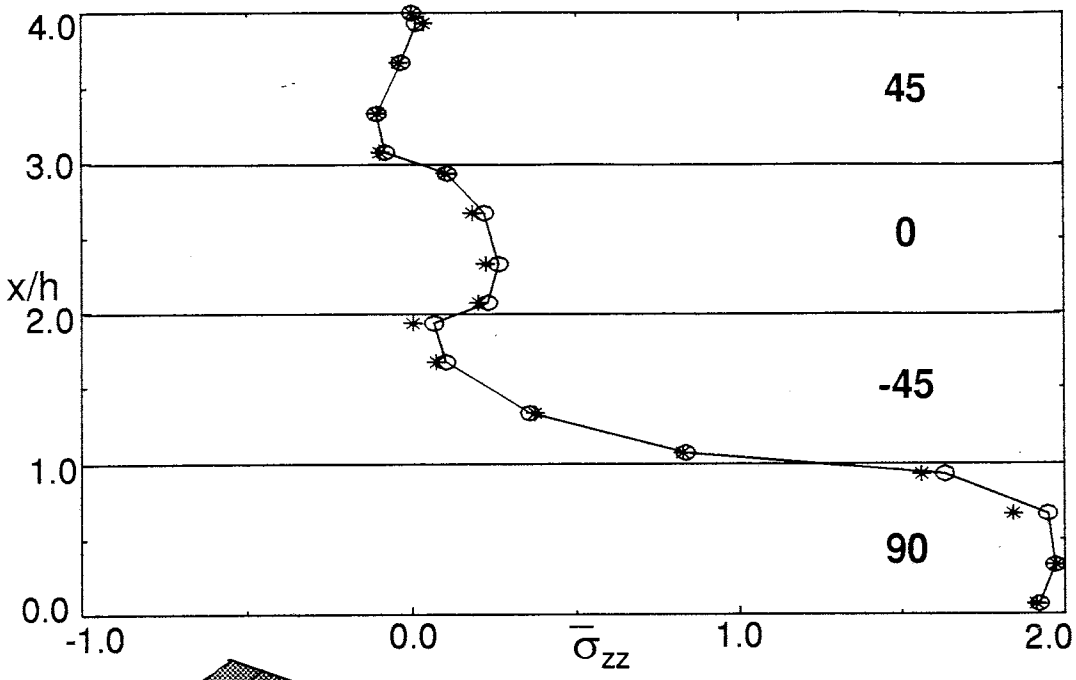


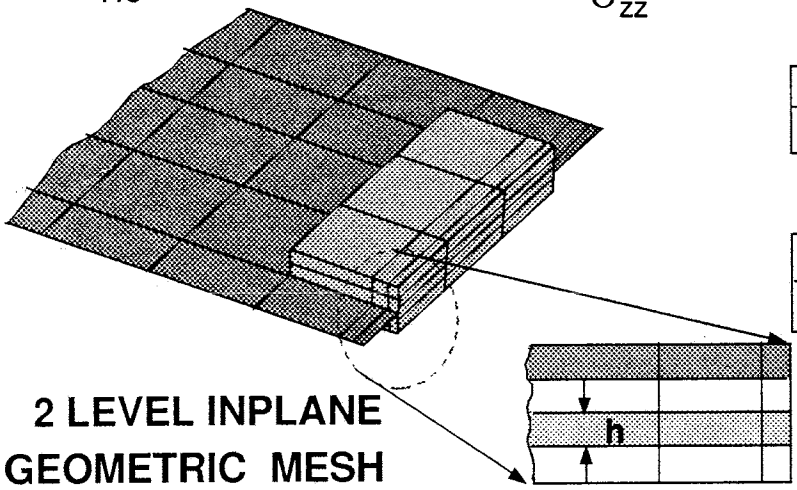


2 LEVEL INPLANE GEOMETRIC MESH

| GLOBAL POLYNOMIAL ORDER = 2 |
|---|
| LOCAL POLYNOMIAL ORDER = 4 |

| | | |
|---|---|---|
| ○ | UNIFORM REFINEMENT | 2145 DOFS |
| ✶ | SELECTIVE REFINEMENT | 1610 DOFS |

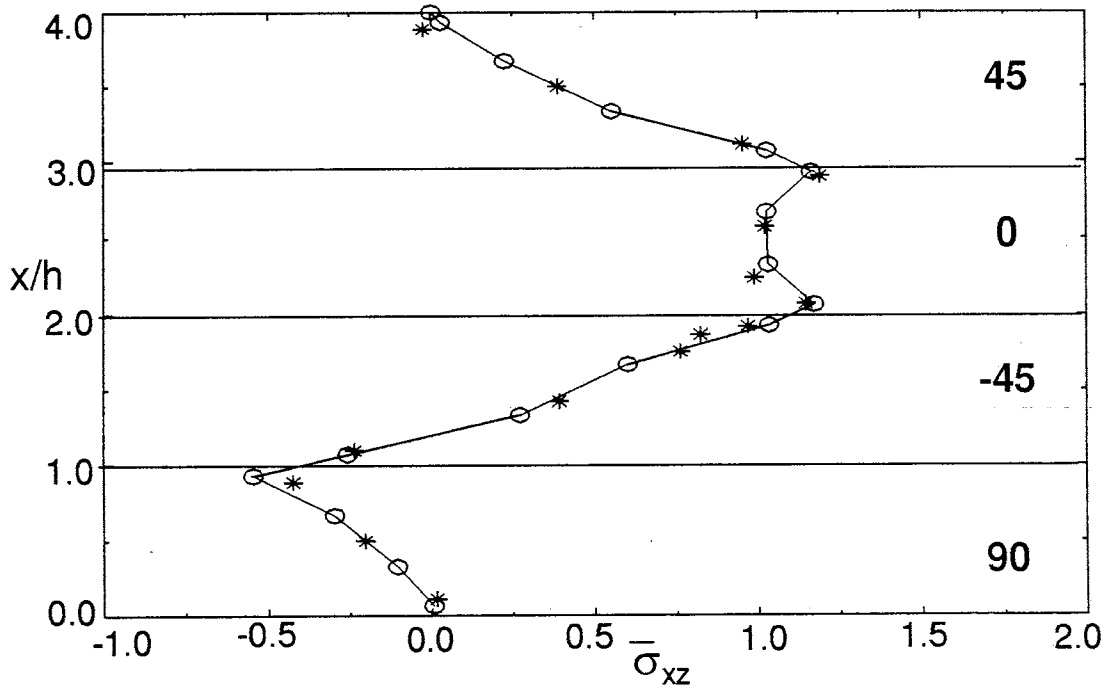


Figure 8

# SCORDELIS-LO ROOF PROBLEM

## ERROR DENSITY DISTRIBUTION

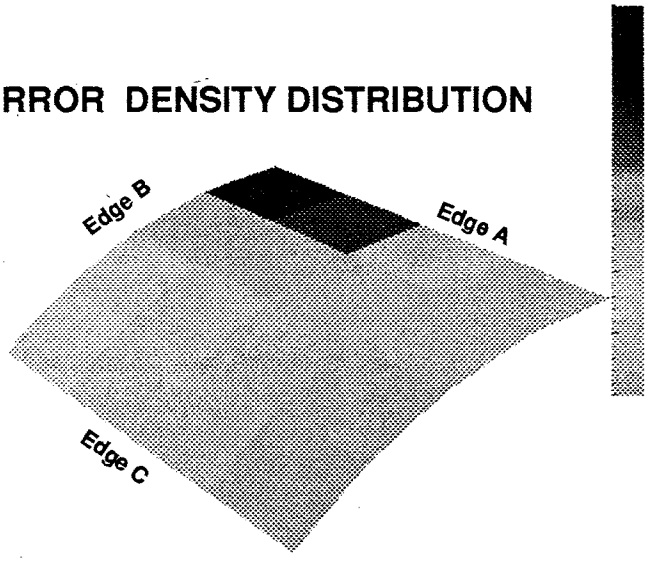


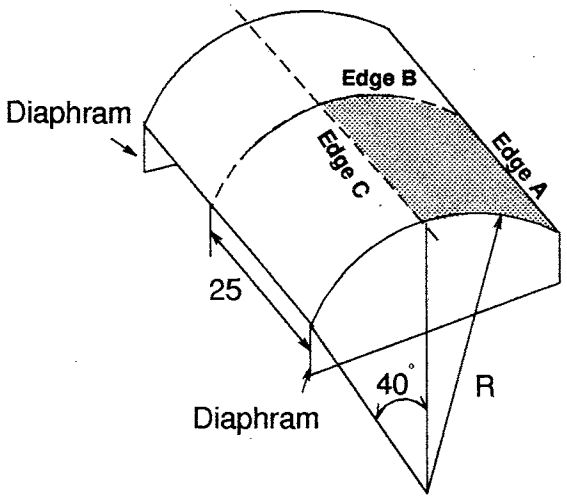


## (45/-45) LAMINATE

$E_1 = 19.5 \times 10^6$ psi,
$E_2 = E_3 = 1.48 \times 10^6$ psi
$G_{12} = G_{13} = 0.80 \times 10^6$ psi,
$G_{23} = 0.49 \times 10^6$ psi
$\nu_{12} = \nu_{13} = 0.30.$
$\nu_{23} = 0.49.$

THICKNESS = 0.25
RADIUS = 25.0
DEAD WEIGHT = 0.333

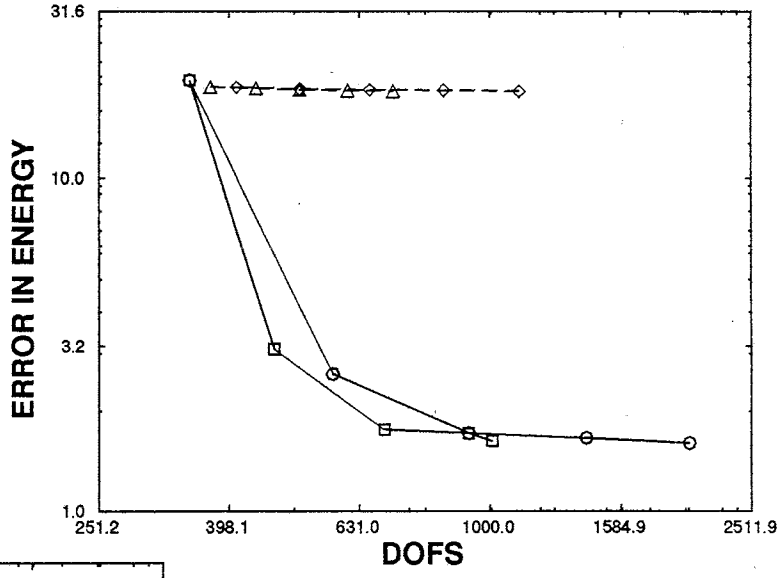


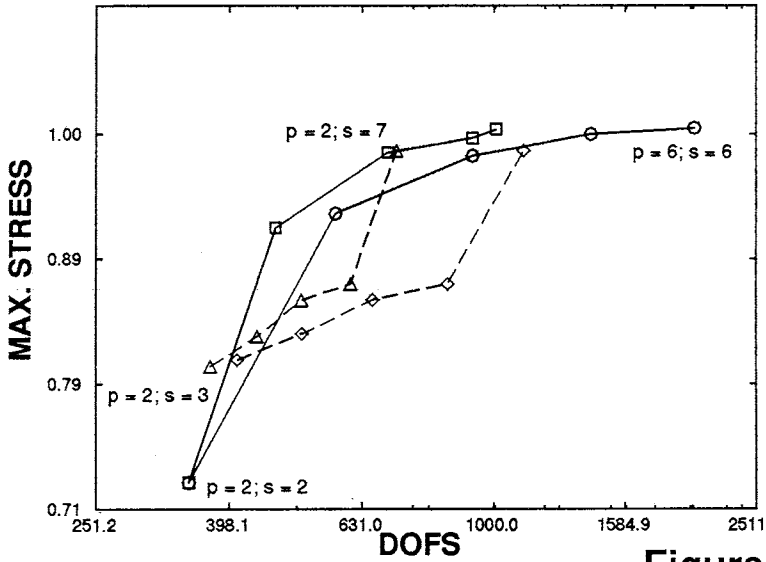


P = POLYNOMIAL ORDER OF GLOBAL MESH
S = POLYNOMIAL ORDER OF LOCAL MESH

| | |
|---|---|
| ○ | UNIFORM POLY ESCALATION<br>P = S = 2..6 |
| □ | SELECTIVE POLY ESCALATION<br>P = S = 2..6 |
| ◇ | UNIFORM POLY ESCALATION<br>P = 2: S= 3..7 |
| △ | SELECTIVE POLY ESCALATION<br>P = 2: S= 3..7 |

Figure 9.

## INTERLAMINAR STRESSES at FREE EDGE
## PARTIAL SUPERPOSITION ON (-45/0) PLYS

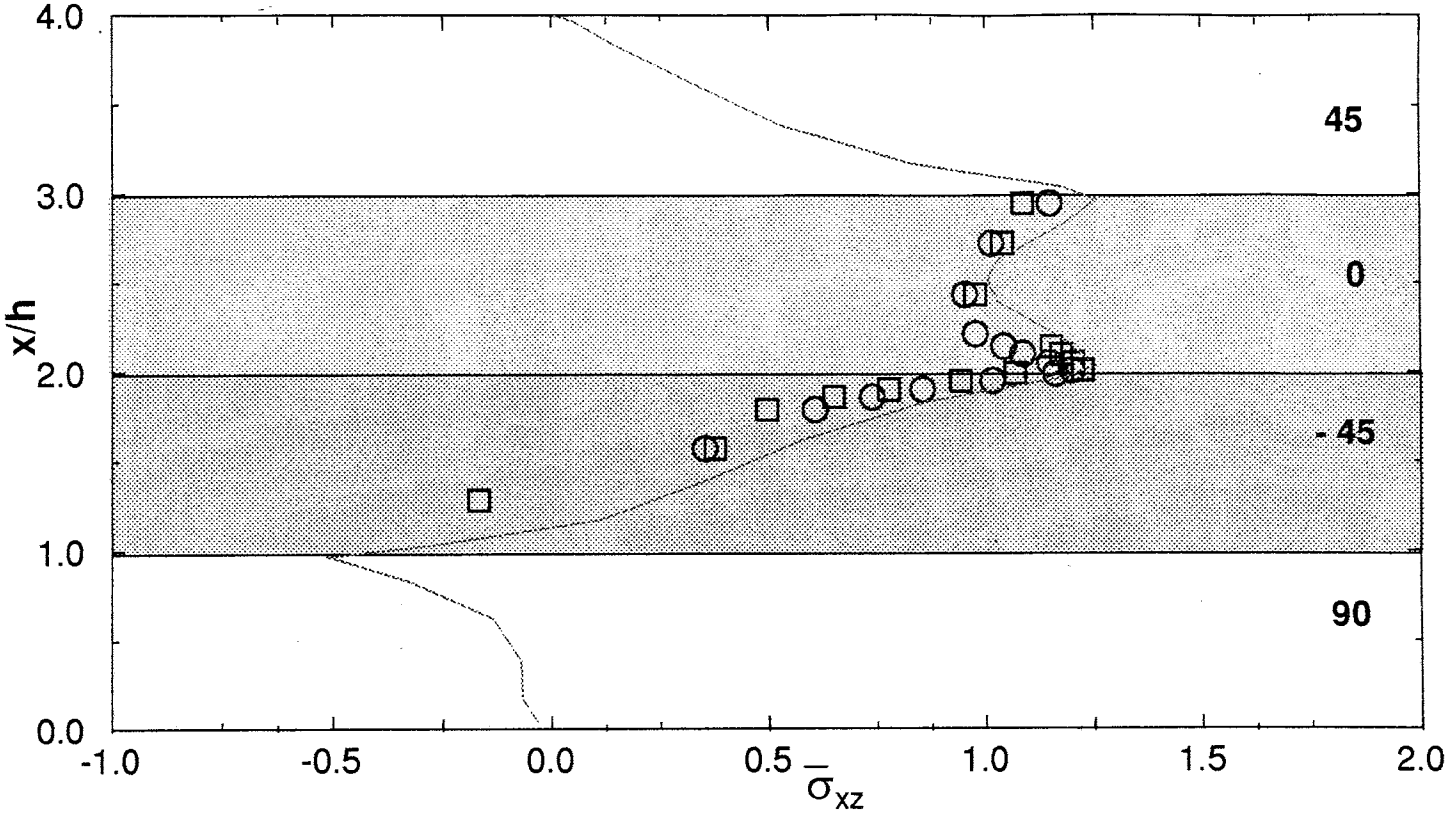


| | | |
|---|---|---|
| ○ | UNIFORM REFINEMENT | 1553 DOFS |
| □ | SELECTIVE REFINEMENT | 1110 DOFS |
| ..... | REFERENCE SOLUTION | |

GLOBAL POLYNOMIAL ORDER = 2
LOCAL POLYNOMIAL ORDER = 4

## PARTIALLY SUPER-IMPOSED MESH

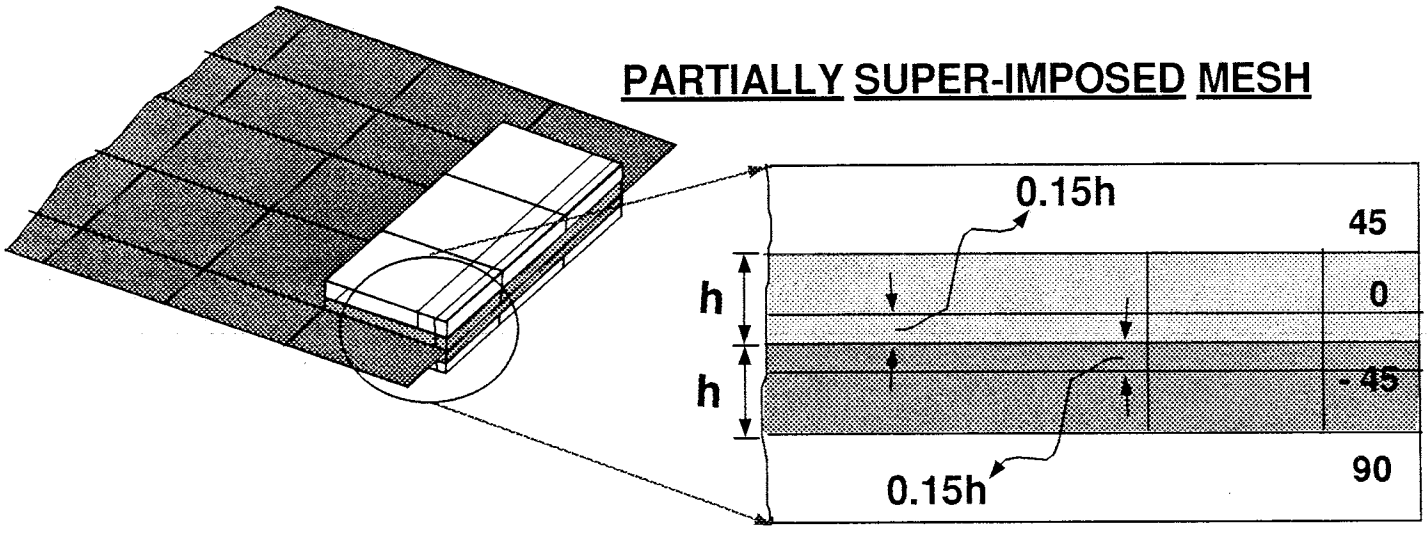


Figure 10

# EDGE DELAMINATION TENSION TEST

$E_1 = 19.5 \times 10^6$ psi,
$E_2 = E_3 = 1.48 \times 10^6$ psi
$G_{12} = G_{13} = 0.80 \times 10^6$ psi,
$G_{23} = 0.49 \times 10^6$ psi
$\nu_{12} = \nu_{13} = 0.30$.
$\nu_{23} = 0.49$.

Figures not to scale

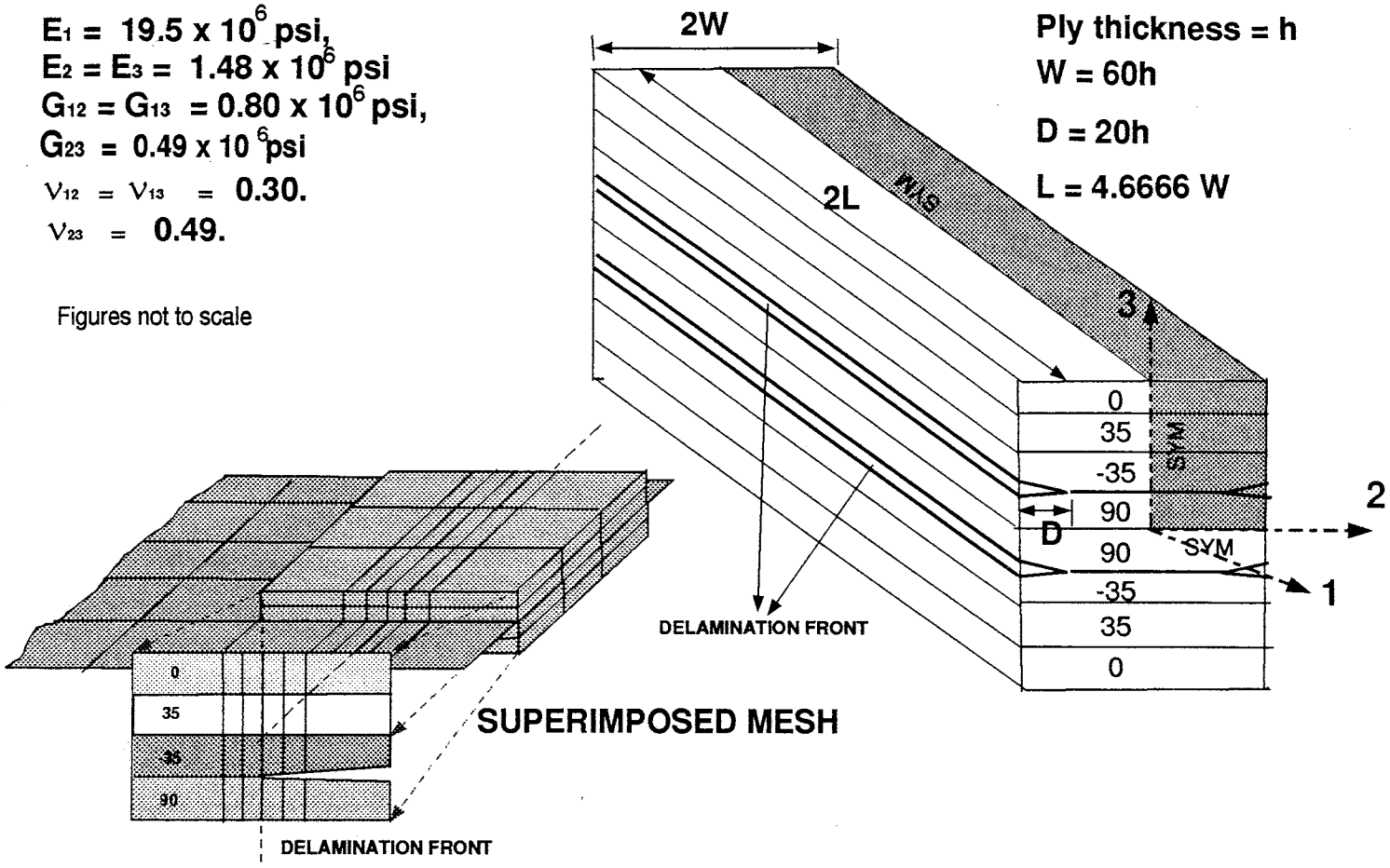


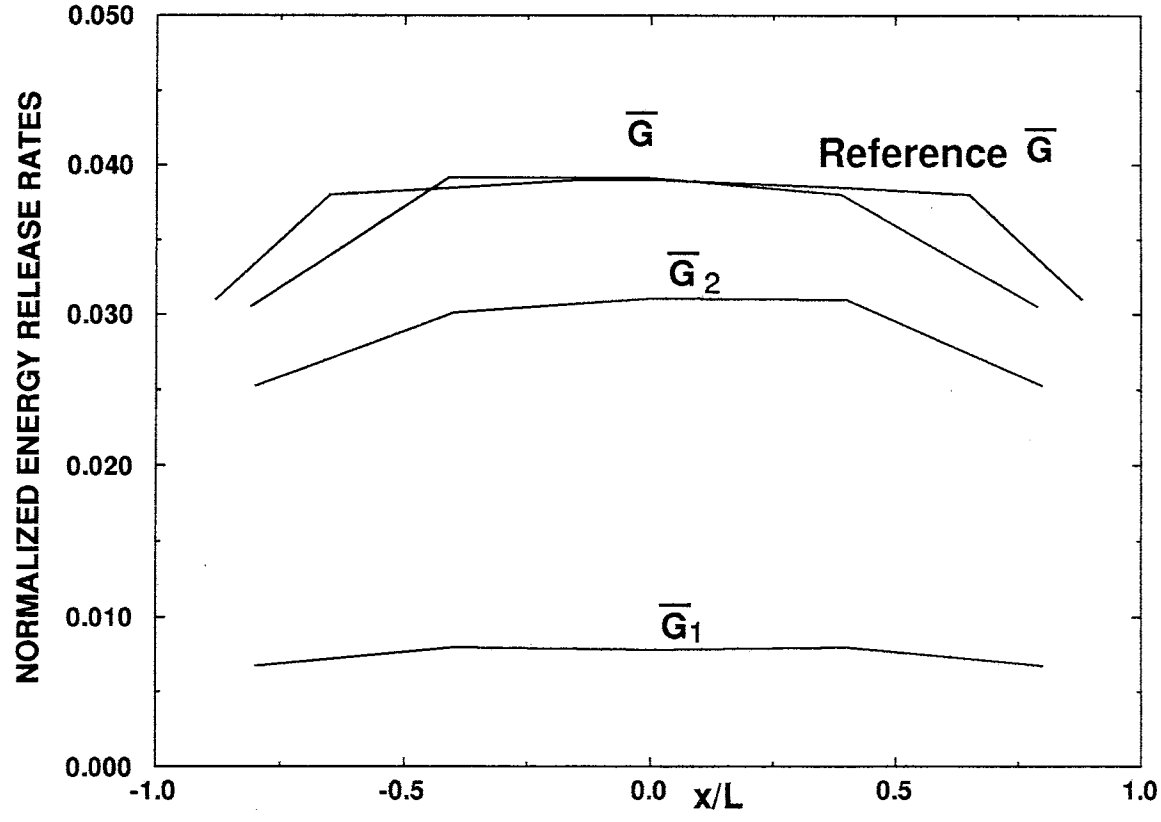


Figure 11

# COMPARISON OF SOLUTION METHODS FOR S-METHOD

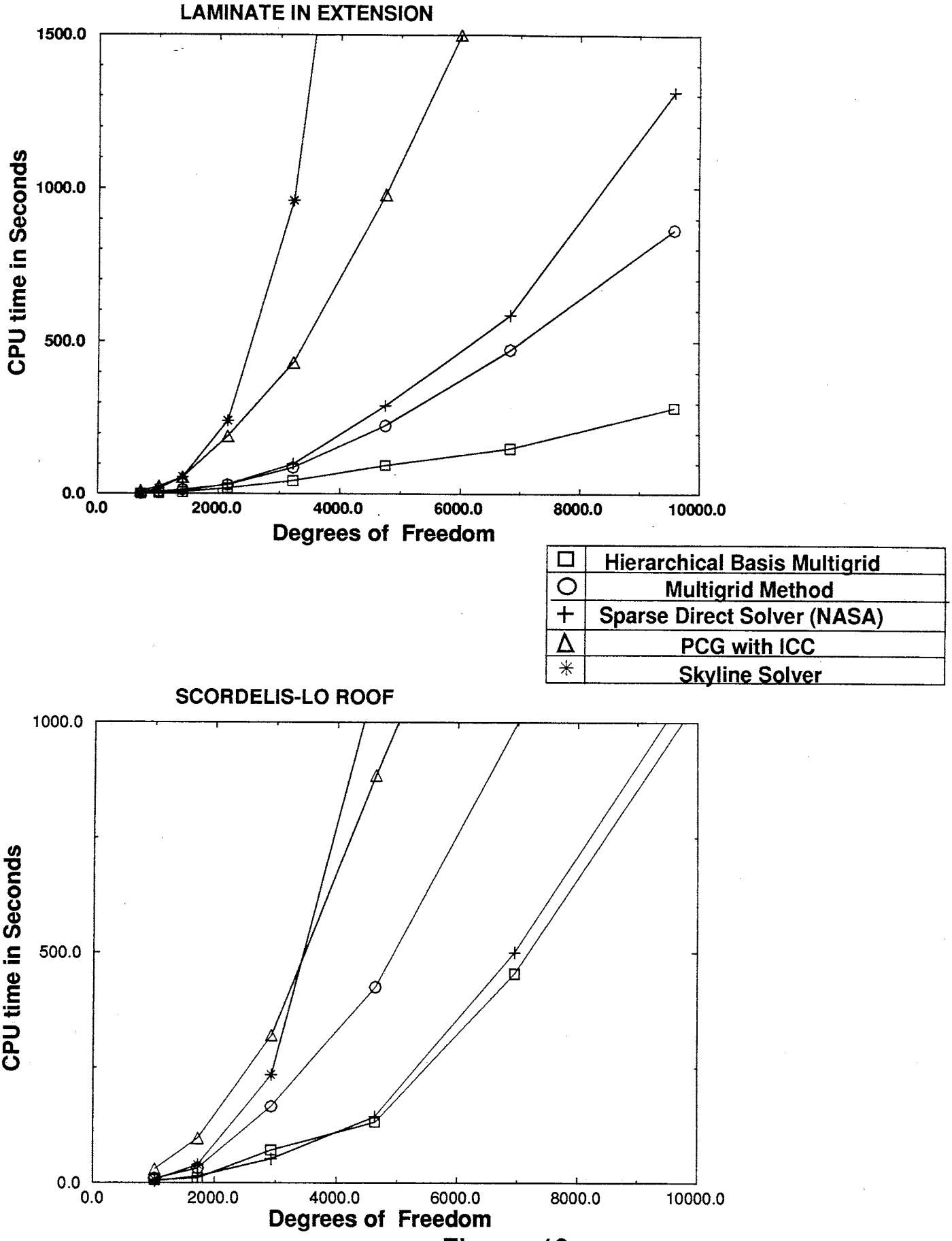


Figure 12.